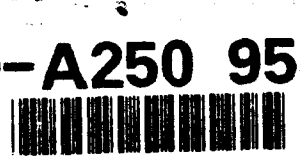

Uniformly valid solutions to the initial-value wavemaker problem

S.W. Joo and W.W. Schultz
Department of Mechanical Engineering and Applied Mechanics

A.F. Messiter
Department of Aerospace Engineering

Contract Number N00014-86-K-0684
Technical Report No. 89-01

January, 1989

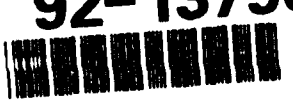

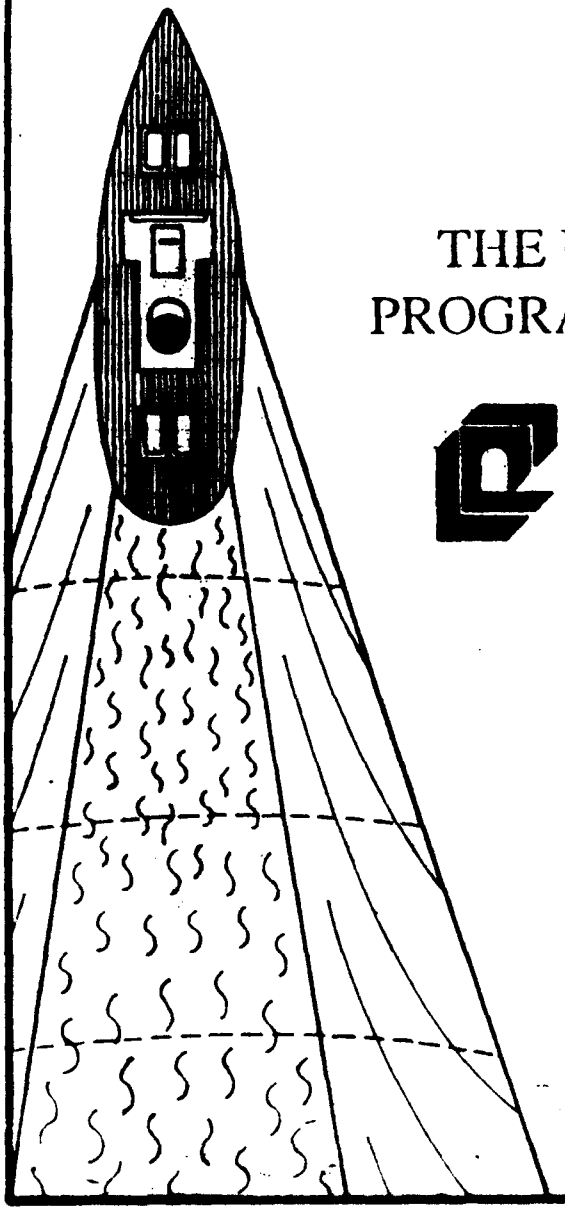

THE UNIVERSITY OF MICHIGAN
PROGRAM IN SHIP HYDRODYNAMICS

COLLEGE OF ENGINEERING

NAVAL ARCHITECTURE &
MARINE ENGINEERING

AEROSPACE ENGINEERING

MECHANICAL ENGINEERING &
APPLIED MECHANICS

SHIP HYDRODYNAMIC
LABORATORY

SPACE PHYSICS RESEARCH
LABORATORY

ERIM

Abstract

A Fourier-integral method is developed to obtain transient solutions to potential wavemaker problems. This method yields solutions that are uniformly valid for wavemaker velocities which need not be given as powers of time. The results are compared with known small-time and local solutions. Examples considered include ramp, step and harmonic wavemaker velocities. As time becomes large, the behavior near the wave front is derived for the impulsive wavemaker, and for the harmonic wavemaker it is shown that the steady-state solution is recovered. The solution for a wavemaker velocity given as a Fourier cosine series compares favorably with the computational and experimental results of Dommermuth et al. (1988). Capillary effects are included and nonlinear effects are discussed.

1 Introduction

The study of water waves associated with surface-piercing bodies has long been an interesting and important area in fluid mechanics. In many cases, however, both analysis and computation run into difficulties near the intersection of a body with the free surface. To examine this problem, a number of researchers have considered a vertical wavemaker moving horizontally in a fluid of finite depth. Peregrine (1972) used a moving coordinate system attached to the wavemaker in his small-time expansion, noted a singular behavior at the contact line, and explained the necessity of a local solution. Chwang (1983) obtained a solution with a stationary coordinate system and argued that the singularity lies outside of the physical domain. However, he did not properly expand the moving wavemaker boundary conditions about the singular point. The logarithmic singularity in the small-time solution was confirmed by Lin (1984) by a Lagrangian description of the problem.

It was not until the work of Roberts (1987) that a successful local solution for the power-law movement of the wavemaker was obtained for small time and small Froude number. He found that for small time the solution varies significantly in the neighborhood of the contact line and gave a self-similar formulation to describe this behavior. If the wavemaker starts to move impulsively ("step velocity"), however, the neglected nonlinear effect becomes important close to the wavemaker, since the linearized vertical velocity becomes infinitely large as time becomes smaller.

The present study approaches the problem using inviscid-flow theory and develops a simple method to obtain solutions that are uniformly valid for wavemaker velocities which need not be given as powers of time. It is also possible to include the effects of surface tension and initial free-surface elevation caused by non-zero static contact angle with little added effort. For viscous fluids the unsteady motion of this contact line, with the no-slip condition incorporated at the body, would require special consideration, as discussed in the review by Dussan V. (1979) and in an application to water waves by Hocking (1987). We will not consider such complications here.

The singularity at the contact line can be shown to be a consequence of an improper expansion. The small-time solution ceases to be a valid asymptotic series in time as the distance from the contact line decreases because the higher-order terms do not remain small. A correct local solution requires a new length scale that varies in time. In other words, very near the contact line spatial variables are coupled with time, so that the small-time expansion does not yield a well-behaved solution there. An alternative to the small-time expansion is an expansion for small Froude number followed by a Laplace transformation, as used by Roberts (1987), or the Fourier transformation used in the present work. Both of these methods can be applied to obtain a solution, since neither requires separation of variables. However, the latter can be more powerful and versatile in that the interpretation of the results and the extension to arbitrary wavemaker velocities are accomplished more easily.

We begin in §2 by introducing the formulation of the vertical wavemaker problem. The velocity of the wavemaker is given as a function of time, and the surface tension on the free surface is retained with non-zero static contact angle.

In §3 and §4 we consider two hypothetical wavemaker velocities, expressed by ramp and step functions in time. The solutions for zero surface tension are shown to agree with the local solutions of Roberts (1987) for small time near the contact line. Also, sufficiently far from the contact line, they are shown to agree with the small-time solution of Peregrine (1972). The nonlinear formulation and large-time behavior for the step velocity are also discussed.

More general types of wavemaker velocities are discussed in §5 and §6. One example is a more realistic velocity that starts from zero and increases toward a finite constant value. It is shown how the solutions for step and ramp velocities can be recovered as limiting cases. In §6, the present method allows a transient solution for a simple-harmonic wavemaker. Sufficiently far from the contact line and in the limit as time approaches infinity, the solution agrees with that of Havelock (1929), as cited by Yih (1979). As a final example in §6, we examine a wavemaker velocity considered by Dommermuth et al. (1988) and compare our analytical solution with their computational and experimental results.

This study is prompted, in part, by computational difficulties caused by bodies intersecting free surfaces. These include small-wavenumber oscillations close to the contact line that may imply a physical or numerical instability. Normally, the spatial dependence is solved by a boundary-integral approach, but these techniques are known to have difficulties with corners, even when singular behavior is not present (Schultz & Hong, 1988). The standard approach is to separate the spatial and temporal behavior, thus introducing singular behavior into the problem as mentioned above, and it is only the inability of the boundary-integral computations to model this apparent singularity that allows the excellent agreement (at least for regions not too close to the wavemaker) of previous computations (Dommermuth et al., 1988).

2 Formulation

We consider the fluid motion due to a moving wall as shown in Fig. 1. If the fluid is inviscid and incompressible, and the motion starts from rest, the flow will be irrotational according to Kelvin's theorem and is described by the Laplace equation. In nondimensional variables

$$\phi_{xx} + \phi_{yy} = 0 \qquad \text{for} \quad x > s(t), \quad -1 < y < \eta(x,t), \tag{1}$$

where $\phi(x,y,t)$ is the velocity potential, $\eta(x,t)$ is the free-surface elevation measured from the undisturbed level at infinity, and $s(t)$ is the displacement of the wall from its initial location, which, of course, is the time integral of the wavemaker velocity. The velocity, length, and time scales are chosen to be $\sqrt{gh}, h, \sqrt{h/g}$, where h is the undisturbed depth of the fluid and g is the gravitational acceleration. The fluid velocity at the wavemaker is prescribed as

$$\phi_x = \alpha u(t) \qquad \text{on} \quad x = s(t), \tag{2}$$

where α is the Froude number. For example, if the dimensional velocity, U, is given by

$$U = C\left(\sqrt{\frac{h}{g}}t\right)^q \qquad t > 0, \tag{3}$$

where C and q are constants, we have

$$\alpha = \frac{C}{\sqrt{g^{1+q}h^{1-q}}}.$$

Thus, $u(t)$ and $s(t)$ in (2) become

$$u(t) = t^q, \qquad s(t) = \alpha t^{q+1}/(q+1).$$

In particular, the cases for $q = 0$ and $q = 1$ correspond to a step velocity and a ramp velocity, respectively.

The aforementioned $u(t)$ describes a power-law movement of the wavemaker, which can approximate the earlier stages of a more general motion for small time and, thus, is frequently used in small-time analyses. In the present work, however, the general expression for $u(t)$ will be maintained and a solution valid for all time will be sought.

In the presence of non-zero surface tension, the kinematic and dynamic boundary conditions on the free surface become

$$\phi_y = \eta_t + \phi_x \eta_x \quad \text{on} \quad y = \eta \tag{4}$$

$$\phi_t + \frac{1}{2}(\phi_x^2 + \phi_y^2) + \eta - \frac{T\eta_{xx}}{(1+\eta_x^2)^{3/2}} = 0 \quad \text{on} \quad y = \eta, \tag{5}$$

where the nondimensional surface tension T, the reciprocal of the Bond number, is defined by

$$T = \frac{\sigma}{\rho g h^2}.$$

Here, σ is the surface-tension constant, and ρ is the density of the fluid. On the bottom, the vertical velocity component vanishes, so that

$$\phi_y = 0 \qquad \text{on} \quad y = -1. \tag{6}$$

Since the motion starts from rest, the initial conditions are

$$\phi = 0 \qquad t < 0 \tag{7}$$

$$\eta = \kappa\sqrt{T}\exp(-\frac{x}{\sqrt{T}}) \qquad t < 0. \tag{8}$$

Here, κ is a constant determined by $\kappa = \tan(\pi/2 - \theta_s)$, where θ_s is the static contact angle. The initial free-surface elevation (8) satisfies the static linear equivalent of (5) for small κ and

becomes zero in the limit as the surface tension becomes zero or the initial contact angle becomes $90°$.

Instead of introducing a small-time expansion, which is not uniformly valid near the contact line, as explained in §1, we now use an expansion for small Froude number. The velocity potential and the free-surface elevation are expanded as

$$\phi(x,y,t) = \alpha\phi_1(x,y,t) + \alpha^2\phi_2(x,y,t) + \cdots \tag{9}$$

$$\eta(x,t) = \kappa\sqrt{T}\exp(-\frac{x}{\sqrt{T}}) + \alpha\eta_1(x,t) + \alpha^2\eta_2(x,t) + \cdots. \tag{10}$$

Although T is typically very small, it is possible to retain $T = O(1)$ in much of the following with very little added complexity.

Expanding the free-surface boundary conditions and the boundary condition on the wavemaker about $y = 0$ and $x = 0$, respectively, gives the equations to leading order, $O(\alpha)$, as

$$\phi_{1xx} + \phi_{1yy} = 0 \qquad \text{for} \quad x > 0, \quad -1 < y < 0 \tag{11}$$

$$\phi_{1x} = u(t) \qquad \text{on} \quad x = 0 \tag{12}$$

$$\phi_{1y} = \eta_{1t} \qquad \text{on} \quad y = 0 \tag{13}$$

$$\phi_{1t} + \eta_1 - T\eta_{1xx} = 0 \qquad \text{on} \quad y = 0 \tag{14}$$

$$\phi_{1y} = 0 \qquad \text{on} \quad y = -1. \tag{15}$$

The boundary condition (12) requires the distance $s(t)$ to be small, so that a restriction should be imposed on t, depending on the velocity $u(t)$. For the step velocity, for example, the condition is $t \ll (1/\alpha)$. This constraint could be relaxed by applying a simple coordinate transformation $x' = x - s(t)$ to fix the location of the wavemaker at $x' = 0$, which leaves the first-order equations (11)-(15) unchanged. However, for large time it should be expected that the cumulative effect of omitted nonlinear terms will no longer be negligible, and that η_2 and ϕ_2 will become large. For example, since the nondimensional wave speed in shallow water is $dx/dt = 1 + O(\alpha)$, we may anticipate that the expansions (9) and (10) are valid for large t only if αt is small.

In solving (11)-(15), we first decompose ϕ_1 into two parts:

$$\phi_1 = 2u(t)\sum_{n=0}^{\infty}\frac{1}{k_n^2}e^{k_n z}\sin k_n y + \phi_1^*(x,y,t), \tag{16}$$

where $k_n = (n+\frac{1}{2})\pi$. The series on the right-hand side satisfies the Laplace equation and all the boundary conditions except on the free surface, where it becomes zero. The remaining term ϕ_1^*, then, can be considered as a correction that enables the complete solution to satisfy appropriate free-surface boundary conditions. Substitution of (16) into (11)-(15) yields

$$\phi_{1xx}^* + \phi_{1yy}^* = 0 \qquad \text{for} \quad x > 0, \quad -1 < y < 0 \tag{17}$$

$$\phi_{1x}^* = 0 \qquad \text{on} \quad x = 0 \tag{18}$$

$$-\frac{2}{\pi}u(t)\ln(\tanh\frac{\pi x}{4}) + \phi_{1y}^* = \eta_{1t} \qquad \text{on} \quad y = 0 \tag{19}$$

$$\phi_{1t}^* + \eta_1 - T\eta_{1xx} = 0 \qquad \text{on} \quad y = 0 \tag{20}$$

$$\phi_{1y}^* = 0 \qquad \text{on} \quad y = -1. \tag{21}$$

The solution for ϕ_1^* is sought as a Fourier cosine integral:

$$\phi_1^* = \int_0^{\infty} A(k,t)\cosh k(y+1)\cos kx\,dk, \tag{22}$$

which already satisfies (17), (18), and (21). The solution for η_1 is then also a Fourier cosine integral:

$$\eta_1 = \int_0^{\infty} B(k,t)\cos kx\,dk. \tag{23}$$

Substituting the representations (22) and (23) into the free-surface conditions (19) and (20) and eliminating B gives

$$A_{tt}\cosh k + k(1+Tk^2)A\sinh k = -\frac{2u(t)}{\pi}(\frac{1}{k}+Tk)\tanh k, \tag{24}$$

by making use of

$$\int_0^{\infty}\tanh k\cos kx\frac{dk}{k} = -\ln(\tanh\frac{\pi x}{4}) \tag{25}$$

(Gradshteyn & Ryzhik, 1980). Equation (24) has a general solution

$$A = A_p(k,t) + c_1(k)\sin\beta t + c_2(k)\cos\beta t, \tag{26}$$

where

$$\beta = \sqrt{k(1 + Tk^2)\tanh k}.$$

Here, A_p is a particular solution of (24) for a given $u(t)$, and c_1 and c_2 are to be determined from the initial conditions.

The Laplace equation does not require any initial condition. Since the time derivatives appear only in the free-surface boundary conditions, the initial conditions are applied on the free surface. The initial condition for η, (8), is converted into a condition for ϕ through (5). Using (9)-(10) again, we then obtain

$$\phi_1 = 0 \qquad \text{and} \qquad \phi_{1t} = 0$$

at $y = 0$ and $t = 0$. Since the series in (16) is always zero at $y = 0$, through (22)

$$A(k,0) = A_t(k,0) = 0. \tag{27}$$

The solution (26), then, is completely determined, and so is ϕ_1^*.

Once ϕ_1^* is obtained, the first-order free-surface elevation, η_1, is given either by (19) or by (20). The vertical velocity,

$$\phi_{1y} = -\frac{2}{\pi}u(t)\ln(\tanh\frac{\pi x}{4}) + \int_0^\infty k\,A(k,t)\sinh k\,\cos kx\,dk,$$

has a logarithmic singularity in the first term, which is cancelled by the same singularity in the second term. This will be examined in greater detail for each specific case in the following sections.

The higher-order velocity potentials also satisfy the Laplace equation with a Neumann condition on the wavemaker, so that the same Fourier-integral method as for ϕ_1 can be used. However, in most cases we do not evaluate the Fourier integral for ϕ_1 or η_1 to obtain exact closed-form solutions. Thus, the nonhomogeneous terms in the higher-order analysis contain some products of Fourier integrals, which makes numerical analysis inevitable except for certain cases.

3 Ramp velocity

The power-law behavior of the wavemaker, as given by (3), deserves special attention, because it can expose the initial evolution of the fluid motion without unnecessary complication. Due to the obvious distinction between the ramp and step velocities, separate consideration will be given to each case.

The ramp velocity represents a wavemaker that starts from rest and increases in speed linearly with time. It corresponds to the case when $q = 1$ in (3), so that the Froude number, α, and the dimensionless velocity, u(t), in (2) become

$$\alpha = \frac{C}{g} \qquad \text{and} \qquad u(t) = t. \tag{28}$$

Therefore, the expansions in (9)-(10) require small acceleration of the wavemaker.

Application of the Fourier-integral method explained in the previous section yields (24) with $u(t) = t$. The solution satisfying (27) is

$$A(k,t) = -\frac{2}{\pi}\frac{1}{k^2 \cosh k}\left(t - \frac{\sin \beta t}{\beta}\right). \tag{29}$$

Then, from (22) and (16), the first-order velocity potential is obtained as

$$\phi_1 = 2t \sum_{n=0}^{\infty} \frac{1}{k_n^2} e^{-k_n x} \sin k_n y - \frac{2}{\pi}\int_0^{\infty} \left(t - \frac{\sin \beta t}{\beta}\right) \frac{\cosh k(y+1)}{\cosh k} \cos kx \, \frac{dk}{k^2}. \tag{30}$$

The vertical velocity of the fluid on the free surface, or the left-hand-side of (19), becomes

$$\phi_{1y} = \frac{2}{\pi}\int_0^{\infty} \frac{\sin \beta t}{\beta} \tanh k \cos kx \, \frac{dk}{k}, \tag{31}$$

where the logarithmic term arising from the infinite series has been cancelled with the help of (25). The free-surface elevation obtained by using (19) is

$$\eta = \frac{2\alpha}{\pi}\int_0^{\infty} \frac{1 - \cos \beta t}{k^2(1 + Tk^2)} \cos kx \, dk + O(\alpha^2) \tag{32}$$

when $\kappa = 0$.

To recover the small-time solution, we can rewrite (32) as the sum of an integral from zero to K and an integral from K to infinity, with K chosen such that $1 \ll K \ll (1/t^2)$. For

$0 \le k \le K$, $\cos\beta t$ can be expanded in a Taylor series in time, whereas for $K \le k < \infty$ we have $\tanh k = 1 + O(e^{-k})$. Then, in the absence of surface tension ($T = 0$), (32) can be expanded as $t \to 0$ with x fixed to give

$$\eta = -\frac{\alpha t^2}{\pi}\ln(\tanh\frac{\pi x}{4}) + \frac{\alpha t^4}{24}\frac{x}{\sinh\frac{\pi x}{2}} + \frac{\alpha t^6}{360\pi}\left[-\frac{1}{x^2} + \int_0^\infty k(\tanh^3 k - 1)\cos kx\,dk\right] + \cdots. \quad (33)$$

The first term in (33) is consistent with the small-time solution of Peregrine (1972) and Chwang (1983), and the additional terms can be obtained by extending the small-time expansion to $O(\alpha t^6)$.

If both x and t are small, with $x = O(t^2)$, the integral (32) can be simplified when $T = 0$ by the addition and subtraction of $\frac{1}{2}kt^2\tanh k$ in the numerator of the integrand. The logarithmic term is obtained explicitly by the use of (25), and the remaining integral is written in two parts as before. It is found that

$$\eta = -\frac{\alpha t^2}{\pi}\ln\frac{\pi x}{4} - \frac{2\alpha t^2}{\pi}\int_0^\infty \left(\frac{1}{2} - \frac{1-\cos\sqrt{k}t}{kt^2}\right)\cos kx\,\frac{dk}{k} + \cdots \quad (34)$$

(Joo et al., 1988), where the integral is a function of x/t^2. Using integration by parts, we find the largest term to be $t^4/(720x^2)$ as $x/t^2 \to \infty$, which agrees with the expansion of (33) as $x \to 0$. The velocity components can be found in a similar way. In complex form, with $z = x + iy = O(t^2)$ as $t \to 0$,

$$\phi_x - i\phi_y = i\frac{2\alpha t}{\pi}\left[\ln\frac{\pi z}{4} + \int_0^\infty \left(\frac{1}{k} - \frac{\sin\sqrt{k}t}{k^{3/2}t}\right)e^{-ikz}dk\right] + \cdots, \quad (35)$$

This result can, of course, be obtained directly by replacing $\tanh(\pi x/4)$ with $\pi x/4$ in (19); the differential equation (24) for A then has $\cosh k$ replaced by 1 and $\sinh k$ by k.

The behavior of the local solution obtained as $z/t^2 \to 0$ is more complicated. To expand the integral in (35) it is convenient to evaluate the following two integrals separately:

$$I_1 = \int_0^\infty \left[(e^{-ikz} - 1) + (1 - \frac{\sin\sqrt{k}t}{\sqrt{k}t})\right]\frac{dk}{k}$$

$$I_2 = -\int_0^\infty (e^{-ikz} - 1)\frac{\sin\sqrt{k}t}{k^{3/2}t}\,dk.$$

The integral I_1 contains a term that cancels the logarithmic term in (35). In I_2, repeated integration by parts provides a power series in z/t^2. Another kind of term appears when $\sqrt{k}\,t$ and kz are

both large and of the same order. This contribution is found by changing the integration contour and choosing the path of steepest descent from $k = t^2/(4z^2)$. Substituting these approximations into (35) finally gives

$$\begin{aligned}\phi_x - i\phi_y &= \alpha t + i\frac{2\alpha t}{\pi}\left(\ln\frac{\pi t^2}{4} + \gamma - 2\right) - \frac{4\alpha t}{\pi}\left[\frac{z}{t^2} + i(\frac{z}{t^2})^2 + \cdots\right] \\ &\quad + \left[-\frac{8\alpha t}{\sqrt{\pi}}(\frac{z}{t^2})^{3/2}\exp\{i(\frac{t^2}{4z} - \frac{\pi}{4})\} + \cdots\right] + \cdots, \end{aligned} \tag{36}$$

for $t \to 0$ and $z/t^2 \to 0$, where $\gamma = 0.577\cdots$ is the Euler constant. The corresponding local solution for the surface elevation is

$$\eta = -\frac{\alpha t^2}{\pi}\left[(\ln\frac{\pi t^2}{4} + \gamma - 3) + \pi(\frac{x}{t^2}) + 2(\frac{x}{t^2})^2 + \cdots\right] - \frac{16\alpha t^2}{\sqrt{\pi}}(\frac{x}{t^2})^{5/2}\cos(\frac{t^2}{4x} - \frac{\pi}{4}) + \cdots + O(\alpha^2). \tag{37}$$

This result is identical to that of Roberts (1987) except that the term $\ln(\pi t^2/4)$ replaces $\ln t^2$. This discrepancy is due to the difference in the problems: Roberts (1987) considered an infinitely deep fluid with a finite-depth wavemaker, $-1 < y < 0$

One important implication of (32) concerns the behavior of the dynamic contact angle between the free surface and the moving wall. This is of particular interest for realistically small values of the nondimensional surface tension T. As $T \to 0$ it is obvious from (20) that a singular-perturbation problem arises near the contact line. The solution to this problem can be recovered from (32). Differentiation of (32) with respect to x and introduction of the transformation $\tilde{k} = kx$ yields

$$\eta_{1x} = -\frac{2}{\pi}\int_0^\infty \left[1 - \cos(\sqrt{\tilde{k}(1 + T\frac{\tilde{k}^2}{x^2})}\frac{t}{\sqrt{x}})\right]\frac{\sin\tilde{k}\,d\tilde{k}}{\tilde{k}(1 + T\frac{\tilde{k}^2}{x^2})},$$

where the $\tanh k$ factor has been replaced by 1 for small x, as in (34). This form is useful for small T, in particular for $T \to 0$ and $x = O(T^{1/2})$. Now if $x/t^2 \to 0$ with $x/T^{1/2}$ fixed, the cosine term in the integrand oscillates rapidly, and the contribution of this term to the integral is small. The remaining term can be integrated to give

$$\eta_x = (\alpha - \kappa)\exp(-\frac{x}{\sqrt{T}}) - \alpha + O(\alpha^2), \tag{38}$$

as $x/t^2 \to 0$ and $T \to 0$ with $x/T^{1/2}$ fixed. Thus, the dynamic contact angle approaches the static contact angle in the limit of zero wavemaker acceleration. However, when the surface tension is zero, (38) becomes $\eta_x = -\alpha$ as $x \to 0$ in agreement with (37). This also agrees with Roberts' (1987) findings and implies a jump in the contact angle at $t = 0$ if T is neglected. For small but nonzero T, the discrepancy is explained by the large curvature $\eta_{xx} = \kappa/\sqrt{T}$ at $x = 0$, as shown by (38).

The integral in (32) is evaluated numerically as the sum of integrals from zero to M and M to infinity. The value for M is chosen to be as large as 10^5 for small x and t, and as small as 10^{-1} when either x or t is large. The integral from zero to M is evaluated using 10-point Gauss-Legendre and 21-point Kronrod formulas on both halves of the adaptive subintervals. The selection of the subinterval is based on the maximum absolute error estimate of 10^{-9}. Due to the rapid oscillation of the integrand, the integral from M to infinity is obtained using Filon's method.

Comparisons of (32) with the small-time solution and the local solution are illustrated in Fig. 2. For small time ($t = 0.1$) and $T = 0$, (32) agrees with the local solution (37) near the wall ($x \ll t^2$), and with the small-time solution (33) sufficiently far from the wall. Fig. 3 shows the free-surface configuration at small time for two different scales when κ is zero. A numerical value of the nondimensional surface tension, T, for pure water at $20°C$ with an undisturbed depth of 1 m is about 0.74×10^{-5}, represented by $T = 10^{-5}$ in Fig. 3. When the surface tension is zero, small-scale waves (or wiggles) can be observed very near the wall, as also noted by Roberts (1987). These wiggles are suppressed in the presence of surface tension, in which case the static contact angle (90° in this case) is retained. At a given time, surface tension also decreases the contact-line elevation. Far from the wavemaker the effect of surface tension becomes less important. These effects become more obvious as we proceed to a step velocity.

4 Step velocity

The wavemaker velocity given by (3) when $q = 0$ is a step velocity, i.e., the wavemaker initially at rest is suddenly set in motion at $t = 0^+$ with a constant velocity.

When the velocity of the wall C is small compared with $\sqrt{gh}$, the expansions in (9)-(10) for small Froude number can be used as before. This time, the Froude number α and the dimensionless velocity $u(t)$ are given as

$$\alpha = \frac{C}{\sqrt{gh}} \qquad \text{and} \qquad u(t) = 1. \tag{39}$$

With $u(t) = 1$, the solution to (24) with the initial conditions in (27) is

$$A(k,t) = -\frac{2}{\pi}\frac{1}{k^2 \cosh k}(1 - \cos \beta t). \tag{40}$$

From (16) and (22),

$$\phi_1 = 2\sum_{n=0}^{\infty} \frac{1}{k_n^2} e^{-k_n x} \sin k_n y - \frac{2}{\pi}\int_0^{\infty} (1 - \cos \beta t)\, \frac{\cosh k(y+1)}{\cosh k} \cos kx\, \frac{dk}{k^2}. \tag{41}$$

After cancellation of the logarithmic terms, The vertical velocity of the free surface becomes

$$\phi_{1y} = \frac{2}{\pi}\int_0^{\infty} \cos \beta t \tanh k \cos kx\, \frac{dk}{k}. \tag{42}$$

Equation (19) then gives the free-surface elevation for $\kappa = 0$ as

$$\eta = \frac{2\alpha}{\pi}\int_0^{\infty} \frac{\beta \sin \beta t}{k^2(1 + Tk^2)} \cos kx\, dk + O(\alpha^2). \tag{43}$$

It is interesting to note that, since the problem is linear, (42) and (43) can be derived directly by differentiating (31) and (32) with respect to time. This procedure is equivalent to Roberts' (1987) use of a convolution integral.

As in the case of a ramp velocity, (43) with $T = 0$ can be shown to agree with

$$\eta = -\frac{2\alpha t}{\pi} \ln(\tanh \frac{\pi x}{4}) + O(\alpha t^3)$$

sufficiently far from the wall, for $x \gg t^2$, and with

$$\begin{aligned} \eta \;=\; & -\frac{2\alpha t}{\pi}\left[(\ln \frac{\pi t^2}{4} + \gamma - 2) - 2(\frac{x}{t^2})^2 + \cdots\right] + \frac{48\alpha t}{\sqrt{\pi}}(\frac{x}{t^2})^{5/2} \cos(\frac{t^2}{4x} - \frac{\pi}{4}) \\ & + \frac{8\alpha t}{\sqrt{\pi}}(\frac{x}{t^2})^{3/2} \sin(\frac{t^2}{4x} - \frac{\pi}{4}) + \cdots + O(\alpha^2) \end{aligned}$$

near the contact line, for $x \ll t^2$. These equations, the small-time solution and the local solution, can be obtained either by tedious analysis or by direct time-differentiation of (33) and (37).

Although the solution procedure differs only slightly from that for the ramp velocity, subtleties arise in the interpretation of (42). If we hold x fixed and let $t \to 0$ in (42), and then let $x \to 0$, the vertical velocity becomes infinitely large, as in the evaluation of (42) for $x/t^2 \gg 1$. If instead we reverse the order in which these two limits are taken, the singular behavior disappears, as can be seen if the expansion of η for $x \ll t^2$ is substituted in (27). The nonuniformity is discussed below.

If (43) is rewritten in terms of $\bar{k} = kx$, it can be shown that $\eta_x = O(\alpha/\sqrt{x})$ as $t, x \to 0$ with x/t^2 fixed. This behavior of η_x is also implied by the expansions for large and small x/t^2. However, since the asymptotic representation requires $|\eta_x| \ll 1$, and therefore $x \gg \alpha^2$, a different inner solution is needed for $t = O(\alpha)$, $x = O(\alpha^2)$. The same conclusion can also be anticipated from dimensional considerations. The relevant parameters for points near the contact line at small time should be C and g rather than g and h, so that the proper reference length and time are $C^2/g = \alpha^2 h$ and $C/g = \alpha(h/g)^{1/2}$, respectively. The corresponding coordinates are t/α and x/α^2.

The correct formulation of an inner problem for small t and x can be shown to require the full nonlinear free-surface conditions. The proper asymptotic form is inferred from the condition that the inner solutions for η, ϕ_x, ϕ_y match with expansions of the previous solutions obtained from (41) and (43) as $x, y, t \to 0$. When (43) is replaced by a representation analogous to (34), it is seen that the largest term in the inner solution for η must match with a term $O(\alpha t \ln \alpha)$. The corresponding y-coordinate should be measured from this first approximation to the surface elevation. Matching the velocities implies that $\phi_x = O(\alpha)$ and $\phi_y = O(\alpha \ln \alpha)$ in the small-scale solution.

The above considerations suggest a solution of the form

$$\phi = (\alpha^3 \ln^2 \alpha)\hat{\phi}_1(\hat{x}, \hat{y}, \hat{t}) + (\alpha^3 \ln \alpha)\hat{\phi}_2(\hat{x}, \hat{y}, \hat{t}) + \alpha^3 \hat{\phi}_3(\hat{x}, \hat{y}, \hat{t}) + \cdots \qquad (44)$$

$$\eta = (\alpha^2 \ln \alpha)\hat{\eta}_1(\hat{x},\hat{t}) + \alpha^2 \hat{\eta}_2(\hat{x},\hat{t}) + \cdots \tag{45}$$

where

$$\hat{x} = \frac{x}{\alpha^2}, \quad \hat{y} = \frac{y - (\alpha^2 \ln \alpha)\hat{\eta}_1(\hat{x},\hat{t})}{\alpha^2}, \quad \hat{t} = \frac{t}{\alpha}.$$

Terms $O(\alpha^2 \ln^4 \alpha)$ in the dynamic free-surface condition (5) give $\hat{\phi}_{1\hat{x}}^2 + \hat{\phi}_{1\hat{y}}^2 = 0$ and so $\hat{\phi}_1 = \hat{\phi}_1(\hat{t})$. Matching gives $\hat{\phi}_{2\hat{x}} \to 0$ and $\hat{\phi}_{2\hat{y}} \to 2/\pi$ as $\hat{x} \to \infty$; since the complex velocity $\hat{\phi}_{2\hat{x}} - i\hat{\phi}_{2\hat{y}}$ is bounded everywhere, it is constant. Terms $O(\alpha^2 \ln^2 \alpha)$ in (5) then give $\hat{\phi}_{1\hat{t}} - \hat{\eta}_{1\hat{t}}\hat{\phi}_{2\hat{y}} + \frac{1}{2}\hat{\phi}_{2\hat{y}}^2 = 0$, where $\hat{\phi}_{2\hat{y}} = 2/\pi$, and so $\hat{\eta}_{1\hat{t}}$ depends only on $\hat{t}$; the kinematic condition (4) shows that $\hat{\eta}_{1\hat{t}} = 2/\pi$. Finally, it follows from (5) that $\hat{\phi}_{2\hat{t}} = -\hat{\eta}_1$. The expansions (44) and (45) therefore become

$$\phi = (\alpha^3 \ln^2 \alpha)\frac{2\hat{t}}{\pi^2} + (\alpha^3 \ln \alpha)\left(\frac{2\hat{y}}{\pi} - \frac{\hat{t}^2}{\pi}\right) + \alpha^3 \hat{\phi}_3(\hat{x},\hat{y},\hat{t}) + \cdots \tag{46}$$

$$\eta = (\alpha^2 \ln \alpha)\frac{2\hat{t}}{\pi} + \alpha^2 \hat{\eta}_2(\hat{x},\hat{t}) + \cdots \tag{47}$$

Conditions to be satisfied by $\hat{\phi}_3$ and $\hat{\eta}_2$ at $\hat{y} = \hat{\eta}_2$ are determined from (4) and (5):

$$\hat{\phi}_{3\hat{t}} + \hat{\eta}_2 + \frac{1}{2}(\hat{\phi}_{3\hat{x}}^2 + \hat{\phi}_{3\hat{y}}^2) = 0 \tag{48}$$

$$\hat{\phi}_{3\hat{y}} - \hat{\eta}_{2\hat{t}} - \hat{\phi}_{3\hat{x}}\hat{\eta}_{2\hat{x}} = 0. \tag{49}$$

That is, the full nonlinear free-surface conditions are required for $\hat{\phi}_3$ and $\hat{\eta}_2$ and are to be evaluated at the unknown location $\hat{y} = \hat{\eta}_2$. The condition (2) at the wavemaker leads to

$$\hat{\phi}_{3\hat{x}} = \hat{t}$$

and is to be evaluated at the actual location of the wall $\hat{x} = \hat{t}$. Thus, the linearized formulation for small Froude number α fails when $t = O(\alpha)$ and $x = O(\alpha^2)$. Here, a full nonlinear problem must be solved, with some added terms involving $\ln \alpha$.

The large-time behavior of the fluid motion is also of interest. The free-surface configuration for large time, but still $t \ll (1/\alpha)$, can be obtained by an asymptotic evaluation of (43). If $\eta = 0$ initially ($\kappa = 0$), the free-surface elevation (43) can be written as

$$\eta = \frac{\alpha}{\pi}\int_0^\infty \sin(\beta t - kx)\frac{\beta\, dk}{k^2(1+Tk^2)} + \frac{\alpha}{\pi}\int_0^\infty \sin(\beta t + kx)\frac{\beta\, dk}{k^2(1+Tk^2)} + \cdots. \tag{50}$$

As $t \to \infty$, the largest contribution to the integrals occurs for small k, at $k = O\{1/(t-x)\}$. If x is not close to t, it is sufficient for a first approximation to replace β by k in the integrand and to omit Tk^2 in the denominator. The result equals α for $x < t$ and zero for $x > t$ (recall that $dx/dt = 1$ corresponds to the speed $\sqrt{gh}$ of a shallow-water wave). This approximation, however, neglects $(k-\beta)t \ll k\,|t-x|$ and therefore fails near the wave front, $x = t$; i.e., since $k - \beta \sim (1-3T)k^3/6$ and $k = O\{1/(t-x)\}$, it has been assumed that $|t-x|^3 \ll t$. When $t - x = O(t^{1/3})$, the cubic term in k must be retained, and the surface elevation becomes

$$\eta = \alpha \int_{\lambda}^{\infty} Ai(\xi)d\xi + \cdots, \tag{51}$$

where $\lambda = (1-3T)^{-1/3}(2/t)^{1/3}(x-t)$ and Ai is the Airy function. For $\lambda > 0$ and $x - t \gg t^{1/3}$, η is exponentially small; for $\lambda < 0$ and $t^{1/3} \ll t - x \ll t$,

$$\eta = \alpha - \frac{\alpha}{\sqrt{\pi t}}\left(\frac{1-3T}{2}\right)^{1/4}\left(1-\frac{x}{t}\right)^{-3/4}\cos\left[\frac{2}{3}\left(\frac{2}{1-3T}\right)^{1/2}t\left(1-\frac{x}{t}\right)^{3/2}+\frac{\pi}{4}\right]+\cdots. \tag{52}$$

When $t - x = O(t)$ behind the wave front, the first integral in (50) has a stationary point at $k = O(1)$ and contributes a term $O(\alpha t^{-1/2})$ that matches with (52). In the second integral there is no stationary point when $x > 0$, and the integration contour can be deformed to lie somewhat away from the real axis in the complex k-plane. The largest contribution is near $k = 0$, giving the value $\pi/2$ with exponentially small error.

Therefore, as time becomes large, the contact-line elevation approaches a value equal to the Froude number, and behind the wave front the free surface can be approximated by a wavetrain superimposed on a flat surface of the same height as the contact line. The amplitude of this wavetrain is $O(\alpha t^{-1/2})$, increasing to $O(\alpha)$ near the wave front. Surface tension increases the frequency and decreases the amplitude decay rate of the wavetrain. Beyond the wave front the free-surface elevation decreases exponentially to the undisturbed value of zero. The width of the wave front increases in proportion to $t^{1/3}$, so that the slope of the free surface near $x = t$ is $O(\alpha t^{-1/3})$.

In Fig. 4, the free-surface elevation is shown at several different times for zero initial elevation ($\kappa = 0$) and for three values of the nondimensional surface tension. Near the wavemaker ($x \ll t^2$),

the free surface is made up of an infinite number of wiggles, which can be approximated by a local solution. Surface tension suppresses these wiggles, but the effects of surface tension are seen to decrease as the distance from the wavemaker increases. This explains why the agreement with experimental measurements (Dommermuth et al., 1988) is good even though surface tension is neglected at moderate distances from the wavemaker. Also shown in Fig. 4e is the asymptotic solution (51) evaluated using the Taylor series and the asymptotic representations in Abramowitz & Stegun (1965), which is in good agreement with the numerical evaluation of the exact solution (43) near the wave front.

The distance from the wavemaker occupied by the wiggles increases with time in agreement with the local solution. The contact-line elevation increases to a maximum, and then oscillates to converge to the Froude number at large time (Fig. 5). Fig. 4d shows that for certain values of time the surface tension actually makes the contact-line elevation higher, as also shown in Fig. 5. The amplitude and frequency of the wiggles near the wavemaker decrease with time until the free surface becomes flat, as indicated by the analysis (50)-(52). The extent of this flat region increases with time, so that in the limit as $t \to \infty$ the behavior of the free surface can be approximated by a hydraulic jump, with the jump location at $x = t$. This corresponds to the phase velocity in shallow water, as can also be seen by imposing conservation laws in a simple control-volume analysis.

5 Exponential wavemaker velocity

As a general example that includes the step and ramp velocities as limiting cases, we consider a wavemaker velocity that has a finite jump in acceleration at $t = 0$ and approaches a constant value U_0 as $t \to \infty$. The exponential form

$$U(t) = U_0 \left[1 - \exp\left(-\sqrt{\frac{h}{g}} \frac{t}{\tau} \right) \right], \tag{53}$$

where τ is a characteristic time, exhibits this behavior. The limits $\tau \to 0$ and $\tau \to \infty$ correspond to the step velocity and the ramp velocity, respectively. The expansions for small Froude number,

(9)-(10), are applied with

$$\alpha = \frac{U_0}{\sqrt{gh}} \qquad \text{and} \qquad u(t) = 1 - e^{-bt}, \tag{54}$$

as the Froude number and nondimensional velocity, respectively. Here $b = \sqrt{h/(g\tau^2)}$. Now, (24) and (27) give

$$A(k,t) = -\frac{2}{\pi}\frac{1}{k^2 \cosh k}\left(1 - \cos\beta t - \beta\frac{\beta e^{-bt} + b\sin\beta t - \beta\cos\beta t}{b^2+\beta^2}\right). \tag{55}$$

Equations (16) and (22) then give the first-order velocity potential as

$$\begin{aligned}\phi_1 \;=\; & 2(1-e^{-bt})\sum_{n=0}^{\infty}\frac{1}{k_n^2}e^{-k_n x}\sin k_n y - \frac{2}{\pi}\int_0^{\infty}\frac{\cosh k(y+1)}{\cosh k}\cos kx \cdot \\ & \cdot\left(1 - \cos\beta t - \beta\frac{\beta e^{-bt} + b\sin\beta t - \beta\cos\beta t}{b^2+\beta^2}\right)\frac{dk}{k^2}.\end{aligned} \tag{56}$$

The vertical velocity on the free surface, after cancellation of the singular terms, becomes

$$\phi_{1y} = \frac{2}{\pi}\int_0^{\infty}\cos\beta t\tanh k\cos kx\frac{dk}{k} - \frac{2}{\pi}\int_0^{\infty}\frac{b^2e^{-bt} - \beta b\sin\beta t + \beta^2\cos\beta t}{b^2+\beta^2}\tanh k\,\cos kx\,\frac{dk}{k}, \tag{57}$$

and the free-surface elevation becomes

$$\eta = \frac{2\alpha}{\pi}\int_0^{\infty}\frac{\beta\sin\beta t}{k^2(1+Tk^2)}\cos kx\,dk + \frac{2\alpha}{\pi}\int_0^{\infty}\frac{be^{-bt} - b\cos\beta t - \beta\sin\beta t}{b^2+\beta^2}\tanh k\,\cos kx\,\frac{dk}{k} + O(\alpha^2). \tag{58}$$

With t fixed, if $b \to 0$, (58) approaches the solution (32) for the ramp velocity with α replaced by αb; if $b \to \infty$, it approaches the solution (43) for the step velocity. The first term in (58) is identical to that for the step velocity, and the other term decays to zero as $t \to \infty$. Consequently, as $t \to \infty$ the behavior of the fluid eventually follows that of the step velocity regardless of the startup process. As $t \to 0$ a special case arises when $b \to \infty$ such that bt becomes constant in the limit—the solution then depends on the value of bt. If $bt \to 0$ or $bt \to \infty$, as $t \to 0$, the small-time solution is recovered for the ramp and the step velocity, respectively.

We have shown in the previous sections that the contact angle of an inviscid fluid remains unchanged from its initial static state in the presence of surface tension. We now examine the

relationship between the acceleration of the wavemaker and the dynamic contact angle when the capillary effect is absent.

When the surface tension is zero ($T = 0$), differentiation of (58) with respect to x and the transformation $\tilde{k} = kx$ yield

$$\eta_x = -\frac{2\alpha}{\pi}\int_0^\infty \left(1 - \frac{\tilde{k}\tanh\frac{\tilde{k}}{x}}{xb^2 + \tilde{k}\tanh\frac{\tilde{k}}{x}}\right)\sqrt{\tilde{k}\tanh\frac{\tilde{k}}{x}}\sin(\sqrt{\tilde{k}\tanh\frac{\tilde{k}}{x}}\frac{t}{\sqrt{x}})\sin\tilde{k}\frac{d\tilde{k}}{\tilde{k}}$$
$$-\frac{2\alpha b}{\pi}\int_0^\infty \left[e^{-bt} - \cos(\sqrt{\tilde{k}\tanh\frac{\tilde{k}}{x}}\frac{t}{\sqrt{x}})\right]\frac{\tanh\frac{\tilde{k}}{x}}{xb^2 + \tilde{k}\tanh\frac{\tilde{k}}{x}}\sin\tilde{k}\,d\tilde{k} + O(\alpha^2). \quad (59)$$

When $x \to 0$ and $x/t^2 \to 0$, this can be evaluated as

$$\eta_x = -\alpha b e^{-bt} + \cdots. \quad (60)$$

Therefore, the slope of the free surface very near the contact line jumps instantaneously to a finite value, which depends on the Froude number and the exponent b, and decays to zero again as time becomes large. Since the decay rate increases with b, it is not surprising to observe the 90° contact angle for the step velocity even at an infinitesimal time (Fig. 4). Since the limit $b \to 0$ corresponds to the ramp velocity for finite time, (60) can easily be shown to be consistent with the previous result, if the difference in definition of the Froude numbers is taken into account.

As shown in the previous section, the linear solution for the step velocity is not valid for very small time, and a fully nonlinear formulation is required. This can be more easily understood by examining the limitation to be imposed on the time constant (or b) for the present wavemaker if the linear solution is to be uniformly valid. As we proceed to the next order, $O(\alpha^2)$, terms proportional to $\alpha^2 b e^{-bt}$ will appear. Then, for $b \gg 1$ the expansions (9)-(10) are valid for all time, including $t \ll (1/b)$ only when $b \ll (1/\alpha)$. If $b = O(1/\alpha)$, nonlinear terms are required when $bt = O(1)$. Therefore, the nonlinear effects cannot be neglected for a rapidly accelerated wavemaker ($\tau = O(U_o/g)$). This is also consistent with (60) when it is combined with the kinematic boundary condition on the free surface (4), which gives the same criterion for the validity of linearisation as above.

The free-surface configurations for various values of b are shown in Fig. 6 when surface ten-

sion and initial free-surface elevation are absent. They resemble those for the ramp velocity when b is small, and those for the step velocity when b is large. As the acceleration of the wavemaker increases (as b becomes larger), the amplitude of the wiggles grows and the contact angle approaches 90°, which is consistent with the above analysis.

6 Harmonic wavemaker velocity

Simple-harmonic motion

A wavemaker motion of greater practical interest is the periodic oscillation, for which the velocity of the wall is given as

$$U(t) = U_0 \sin\left(\sqrt{\frac{h}{g}}\Omega t\right) \qquad t > 0, \tag{61}$$

where U_0 is the maximum velocity of the wall and Ω is the frequency of the oscillation. The well-known linear steady-state solution to this problem was obtained by Havelock (1929) and has been extended by many others. The Fourier-integral method adopted in this study will lead to a transient solution that agrees with the steady-state solution as $t \to \infty$.

The Froude number is defined as in the previous section, and the normalization of the wavemaker velocity gives

$$u(t) = \sin \omega t, \tag{62}$$

where the nondimensional frequency of the wavemaker oscillation is $\omega = \Omega\sqrt{h/g}$, so the solution for (24) that satisfies (27) is now

$$A(k,t) = \frac{2}{\pi}\frac{\beta}{k^2 \cosh k}\frac{\beta \sin \omega t - \omega \sin \beta t}{\omega^2 - \beta^2}. \tag{63}$$

Therefore, the complete first-order velocity potential is

$$\phi_1 = 2 \sin \omega t \sum_{n=0}^{\infty} \frac{1}{k_n^2} e^{-k_n x} \sin k_n y + \frac{2}{\pi}\int_0^{\infty} \frac{\beta(\beta \sin \omega t - \omega \sin \beta t)\cosh k(y+1)}{(\omega^2 - \beta^2)\cosh k} \cos kx \frac{dk}{k^2}. \tag{64}$$

Again, the singular terms in the vertical velocity are cancelled to give

$$\phi_{1y} = \frac{2\omega}{\pi}\int_0^{\infty} \frac{\omega \sin \omega t - \beta \sin \beta t}{\omega^2 - \beta^2} \tanh k \cos kx \frac{dk}{k} \tag{65}$$

on the free surface. The free-surface elevation is then

$$\eta = \frac{2\alpha\omega}{\pi}\int_0^\infty \frac{\cos\omega t - \cos\beta t}{\beta^2-\omega^2}\tanh k\,\cos kx\,\frac{dk}{k} + O(\alpha^2). \tag{66}$$

Far from the wavemaker, the asymptotic evaluation of (66) is possible in the limit as $t \to \infty$. As x and t become large, the largest contribution to the integral in (66) occurs in the neighborhood of $k = k_0$, where k_0 is the positive real root of

$$k_0(1+Tk_0^2)\tanh k_0 = \omega^2. \tag{67}$$

Since this is just the dispersion relation, k_0 is the wavenumber that would be observed for waves with the single frequency ω. Therefore, (66) can be written as

$$\eta = \frac{2\alpha\omega}{\pi}\int_{k_0-\epsilon}^{k_0+\epsilon} \frac{\cos\omega t\,\cos kx - \frac{1}{2}\cos(kx+\beta t) - \frac{1}{2}\cos(kx-\beta t)}{\beta^2-\omega^2}\tanh k\,\frac{dk}{k} + \cdots, \tag{68}$$

where ϵ is a small number such that $1 \ll (1/\epsilon) \ll x$. The integrand in (68) can be expanded about $k = k_0$ and the resulting equation can be easily simplified after setting $(k-k_0)x = \bar{k}$:

$$\begin{aligned}\eta \;=\; & \frac{\alpha\tanh k_0}{\pi k_0 C_g}\int_0^\infty [-2\cos\omega t\,\sin k_0 x\,\frac{\sin\bar{k}}{\bar{k}} \\ & + \sin(k_0x+\omega t)\,\frac{\sin(1+C_gt/x)\bar{k}}{\bar{k}} + \sin(k_0x-\omega t)\,\frac{\sin(1-C_gt/x)\bar{k}}{\bar{k}}]\,d\bar{k} + \cdots.\end{aligned} \tag{69}$$

Here, C_g is the group velocity of the gravity-capillary wave with wave number k_0 and is given by

$$C_g = \frac{(1+3Tk_0^2)\omega^2 + k_0^2(1+Tk_0^2)\mathrm{sech}^2 k_0}{2k_0\omega}. \tag{70}$$

When $x > C_gt$, the approximation (69) is zero; when $x < C_gt$, (69) gives

$$\eta = -\frac{\alpha\tanh k_0}{k_0 C_g}\sin(k_0x-\omega t) + \cdots, \tag{71}$$

which describes the free-surface configuration in a region behind the wave front but far ahead of the wavemaker. In the absence of surface tension ($T = 0$), the approximation (71) agrees with the steady-state solution away from the wavemaker obtained by Havelock (1929). As for the step

velocity, the behavior of the free surface near the wave front ($x = C_g t$) could be obtained by extending the above analysis to higher orders.

The behavior of the contact angle in the absence of surface tension is obtained by differentiating (66) with respect to x and transforming k to $\tilde{k}$ as before, which gives

$$\eta_x = -\frac{2\alpha\omega}{\pi}\int_0^\infty \left[\cos\omega t - \cos\left(\sqrt{\tilde{k}\tanh\frac{\tilde{k}}{x}}\frac{t}{\sqrt{x}}\right)\right]\frac{\tanh\frac{\tilde{k}}{x}}{\tilde{k}\tanh\frac{\tilde{k}}{x} - x\omega^2}\sin\tilde{k}x\,d\tilde{k} + O(\alpha^2).$$

This can be simplified to

$$\eta_x = -\alpha\omega\cos\omega t + \cdots \tag{72}$$

as $x/t^2 \to 0$ and $x \to 0$. The discontinuity in the contact angle at $t = 0$ is consistent with the previous results. It can be easily observed from (72) that the contact angle oscillates with a 90^o phase shift from the wavemaker velocity.

Fig. 7 shows the free-surface configuration at large time for two different wavemaker frequencies. The harmonic wavetrain of Havelock (1929) is observed between the wavemaker and the harmonic-wave front, $x = C_g t$. The amplitude and frequency of this wavetrain can be obtained easily from (67) and (70)-(71). As the undisturbed free surface is approached, ahead of the harmonic-wave front, we observe a second wave front that travels at the maximum phase velocity $dx/dt = 1$, the value for shallow-water waves. The waves between these wave fronts are seen to have decreasing amplitude and wavenumber. The largest change of amplitude occurs near $x = C_g t$ in both Fig. 7a and 7b.

Harmonic analysis of a general wavemaker velocity

As a final example, the velocity of a wavemaker given by a Fourier cosine series

$$u(t) = \sum_{n=1}^{N} a_n \cos(\omega_n t - \theta_n) \tag{73}$$

is considered. A straightforward application of (27) gives

$$A = \frac{2}{\pi}\frac{\beta}{k^2\cosh k}\sum_{n=1}^{N}\frac{a_n}{\omega_n^2 - \beta^2}\left[\omega_n\sin\theta_n\sin\beta t - \beta\cos\theta_n\cos\beta t + \beta\cos(\omega_n t - \theta_n)\right]. \tag{74}$$

We then follow the same procedure as before to obtain

$$\eta = \frac{2\alpha}{\pi} \int_0^\infty \left[\sum_{n=1}^{N} \omega_n \frac{\omega_n \sin(\omega_n t - \theta_n) + \omega_n \sin\theta_n \cos\beta t - \beta \cos\theta_n \sin\beta t}{\omega_n^2 - \beta^2} \right] \tanh k \cos kx \frac{dk}{k} + O(\alpha^2). \tag{75}$$

We take $N = 72$ and $T = 0$ and use the Fourier cosine coefficients of the wavemaker velocity provided by Dommermuth et al. (1988). Fig. 8 compares the free-surface elevations against time at three different locations to the results of Dommermuth et al. (1988) obtained by the boundary-integral method with linearised free-surface conditions. We have chosen to include only the extrema of their figures for clarity. Also shown, when sufficiently different from the linear computations, are their wave-probe measurements. For a moderate distance from the wavemaker (x=3.17), the free-surface elevation (75) shows good agreement with the experimental measurements. Farther away from the wavemaker (x=9.17), the nonlinear effects have accumulated, and the agreement becomes less satisfactory. In all cases, very close agreement is observed between the present Fourier-integral solution and the numerical solution of Dommermuth et al. (1988). Since the linear solution (75) is exact and can be evaluated as accurately as we choose, the small difference between (75) and the numerical solution can be attributed to the difficulties in the boundary-integral computation associated with the contact line. As shown in the previous sections, surface tension affects the free-surface configuration primarily very near the wavemaker ($x \ll t^2$) and for small time, so it is neglected in these comparisons.

7 Concluding remarks

To avoid an artificial singularity at the contact line between the free surface and the wavemaker introduced by the small-time expansion, a Fourier-integral method is developed for small Froude number. This method yields solutions that are uniformly valid for general wavemaker velocities that need not be given as powers of time. It also allows the study of the capillary effects with little added effort.

In the absence of surface tension, an infinite number of small-scale wiggles is present near the wavemaker, as shown also in the local solution of Roberts (1987) for small time, and the contact

angle has a jump at $t = 0$. Surface tension suppresses the wiggles and maintains the contact angle at its initial static value. Far from the wavemaker, effects of surface tension become less important. For consistent and realistic results, surface tension should be considered near the contact line.

When the acceleration of the wavemaker is sufficiently large, the present linear solution is not uniformly valid near the wavemaker for very small time. A correct inner solution for these conditions requires a full nonlinear formulation.

The large-time behavior for the wavemaker moving with constant velocity is also obtained. The contact-line elevation approaches a value equal to the Froude number, and the free surface behind the wave front can be approximated by a wavetrain superimposed on a flat surface. Beyond the wave front, which moves with the phase velocity for shallow water, the free-surface elevation decreases exponentially to the undisturbed value, zero. For the simple-harmonic wavemaker, the large-time behavior agrees with the steady-state solution of Havelock (1929) behind the wave front but far from the wavemaker.

A general wavemaker velocity given by a Fourier cosine series is considered, and the free-surface elevation is compared with the computational and experimental results of Dommermuth et al. (1988). The present Fourier-integral solution agrees very well with the linear numerical results. The agreement with the wave-probe measurements is excellent at moderate distances from the wavemaker for all time and becomes less satisfactory farther away from the wavemaker for large time, when the nonlinear effects have accumulated.

This work was partially supported by the Program in Ship Hydrodynamics at The University of Michigan funded by the University Research Initiative of the Office of Naval Research Contract N000184-86-K-0684, ONR Ocean Engineering Contract N00014-87-0509, and partly (S. W. J) by a Horace H. Rackham Predoctoral Fellowship at The University of Michigan.

REFERENCES

Abramowitz, M., Stegun, I. A. 1965 Handbook of mathematical functions. Dover. 447-449.

Chwang, A. T. 1983 Nonlinear hydrodynamic pressure on an accelerating plate. Phys. Fluids. 25, 383-387.

Dommermuth, D. G., Yue, D. K. P., Chan, E. S., Melville, W. K. 1988 Deep water plunging breakers: a comparison between potential theory and experiments. J. Fluid Mech. 189, 423-442.

Dusan V., E. B. 1979 On the spreading of liquids on solid surfaces: static and dynamic contact lines. Ann. Rev. Fluid Mech. 11, 371-400.

Gradshteyn, I. S., Ryzhik, I. M. 1980 Table of integrals, series, and products. Academic Press, 516.

Havelock, T. H. 1929 Forced surface-waves on water. Phil. Mag. 8, 569-576.

Hocking, L. M. 1987 The damping of capillary-gravity waves at a rigid boundary. J. Fluid Mech. 179, 253-266.

Joo, S. W., Messiter, A. F., Schultz, W. W. 1988 Evolution of nonlinear waves due to a moving wall. 3rd International Workshop on Water Waves and Floating Bodies. Woods Hole, MA.

Lin, W. M. 1984 Nonlinear motion of the free surface near a moving body. Ph.D. thesis, MIT, Dept. of Ocean Engineering.

Peregrine, D. H. 1972 Flow due to a vertical plate moving in a channel. Unpublished note.

Roberts, A. J. 1987 Transient free-surface flows generated by a moving vertical plate. Q. J. Mech. Appl. Math. 40, 129-158.

Schultz, W. W., Hong, S. W. 1989 Solution of potential problems using an overdetermined complex boundary integral method. To appear in J. Comput. Phys.

Yih, C. S. 1979 Fluid Mechanics. West River Press, 195-197.

LIST OF FIGURES

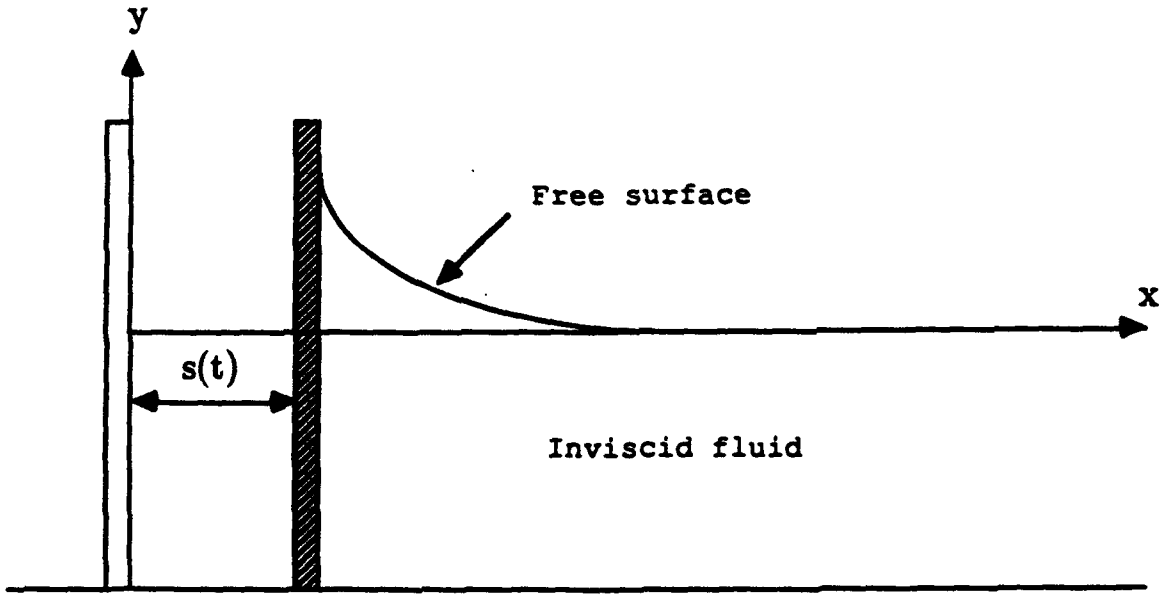

Fig. 1

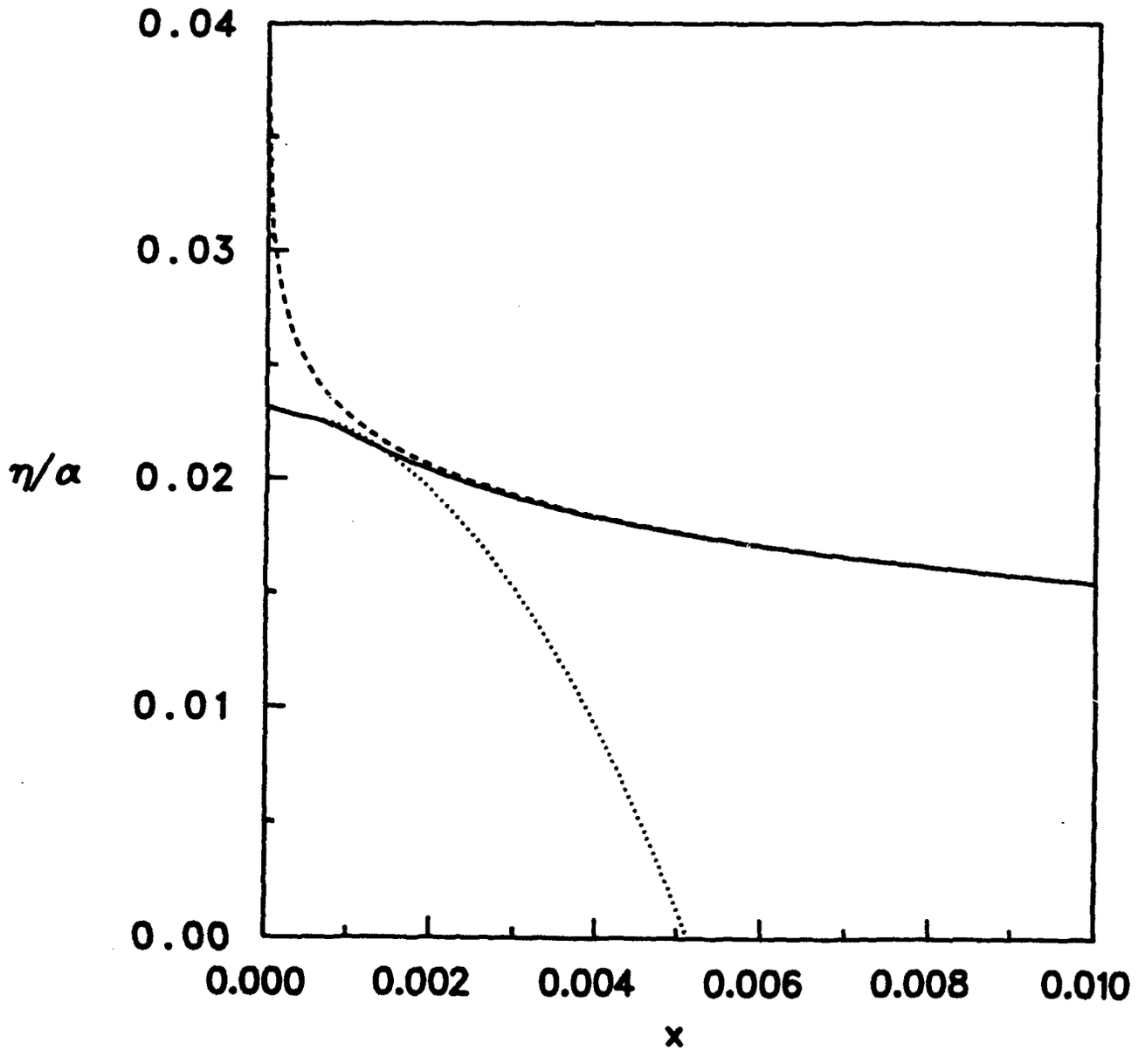

Fig. 2

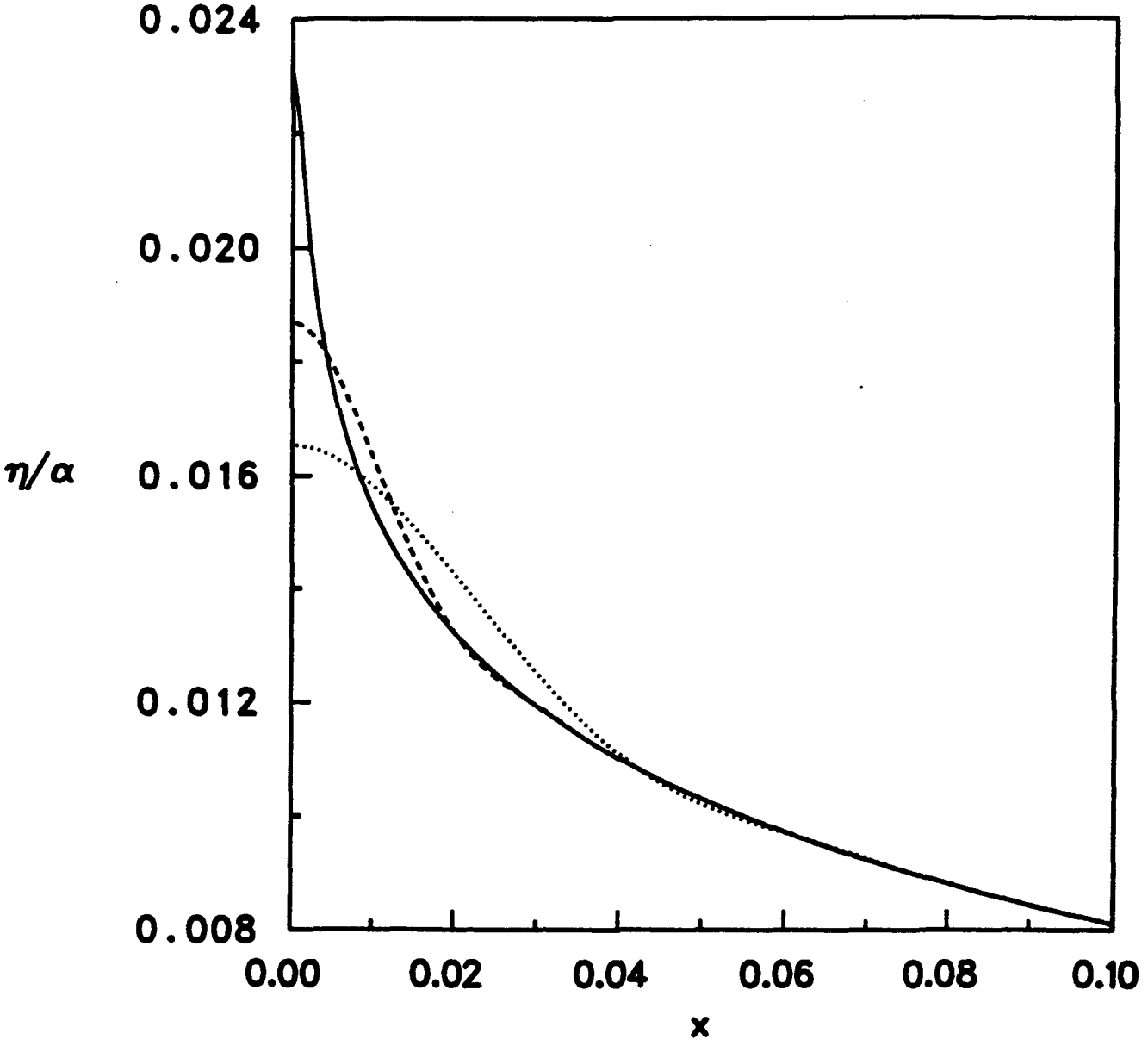

Fig. 3a

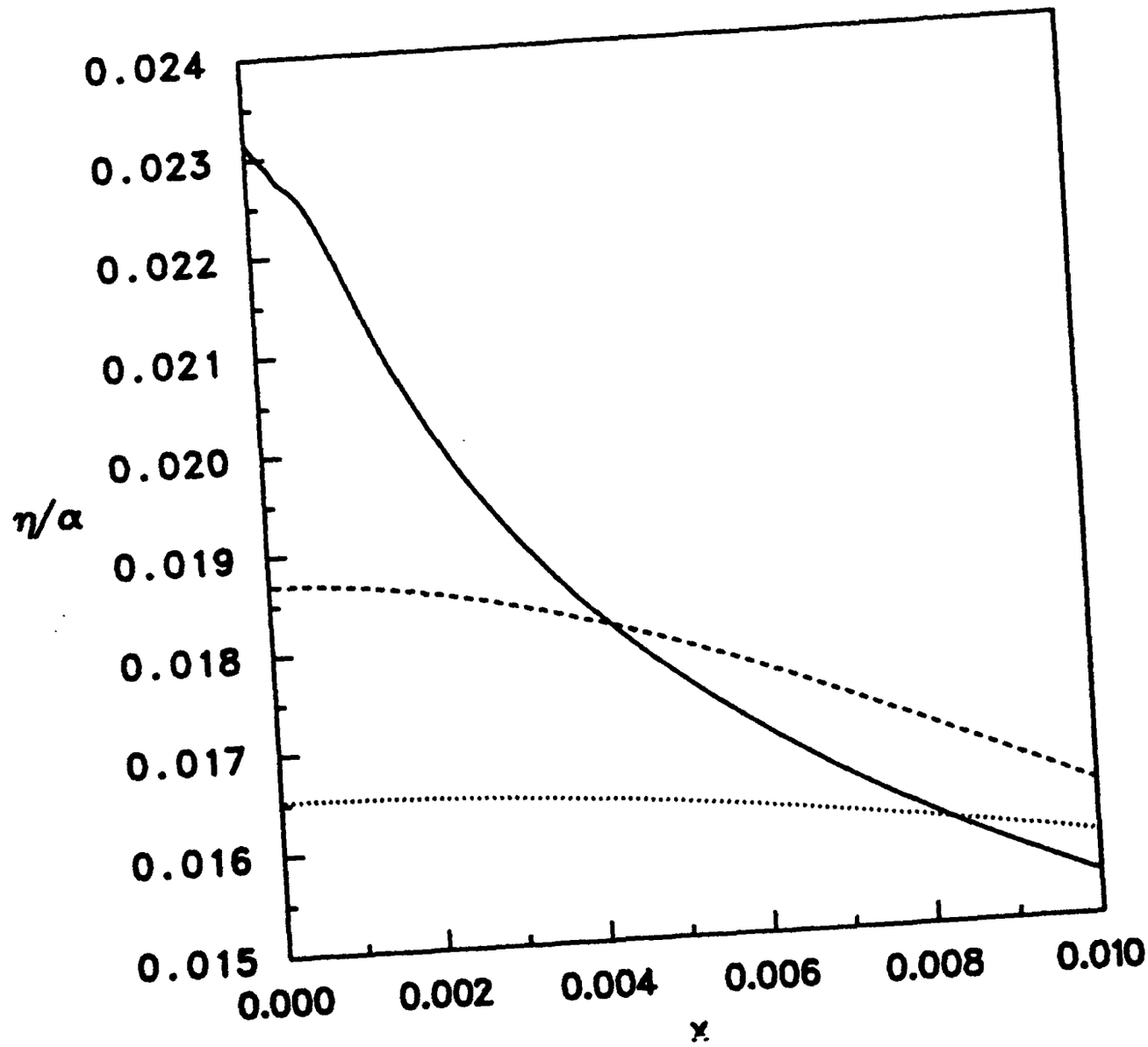
0.024
0.023
0.022
0.021
0.020
η/α
0.019
0.018
0.017
0.016
0.015
0.000
0.002
0.004
0.006
0.008
0.010
x

Fig. 3b

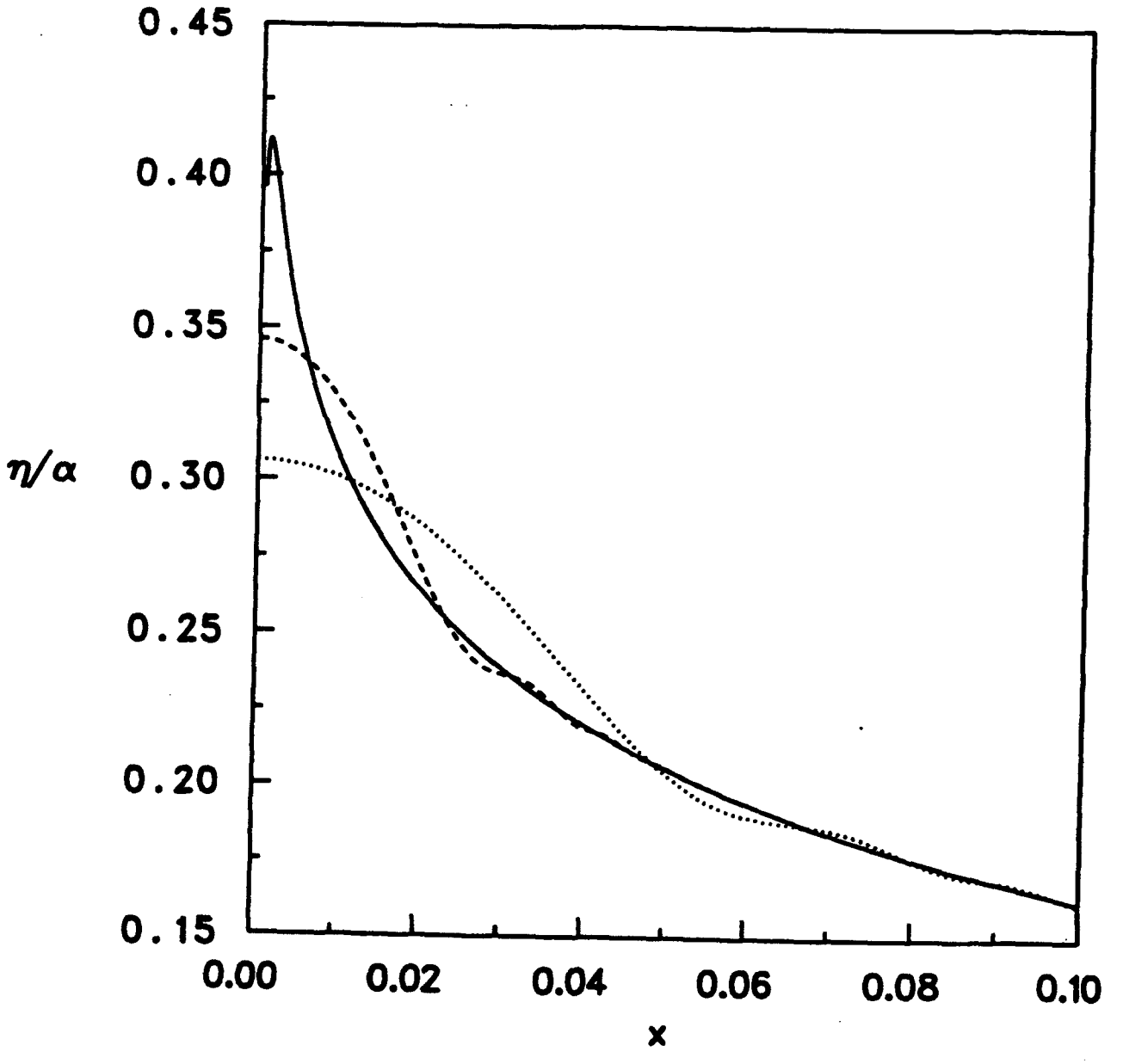

Fig. 4a

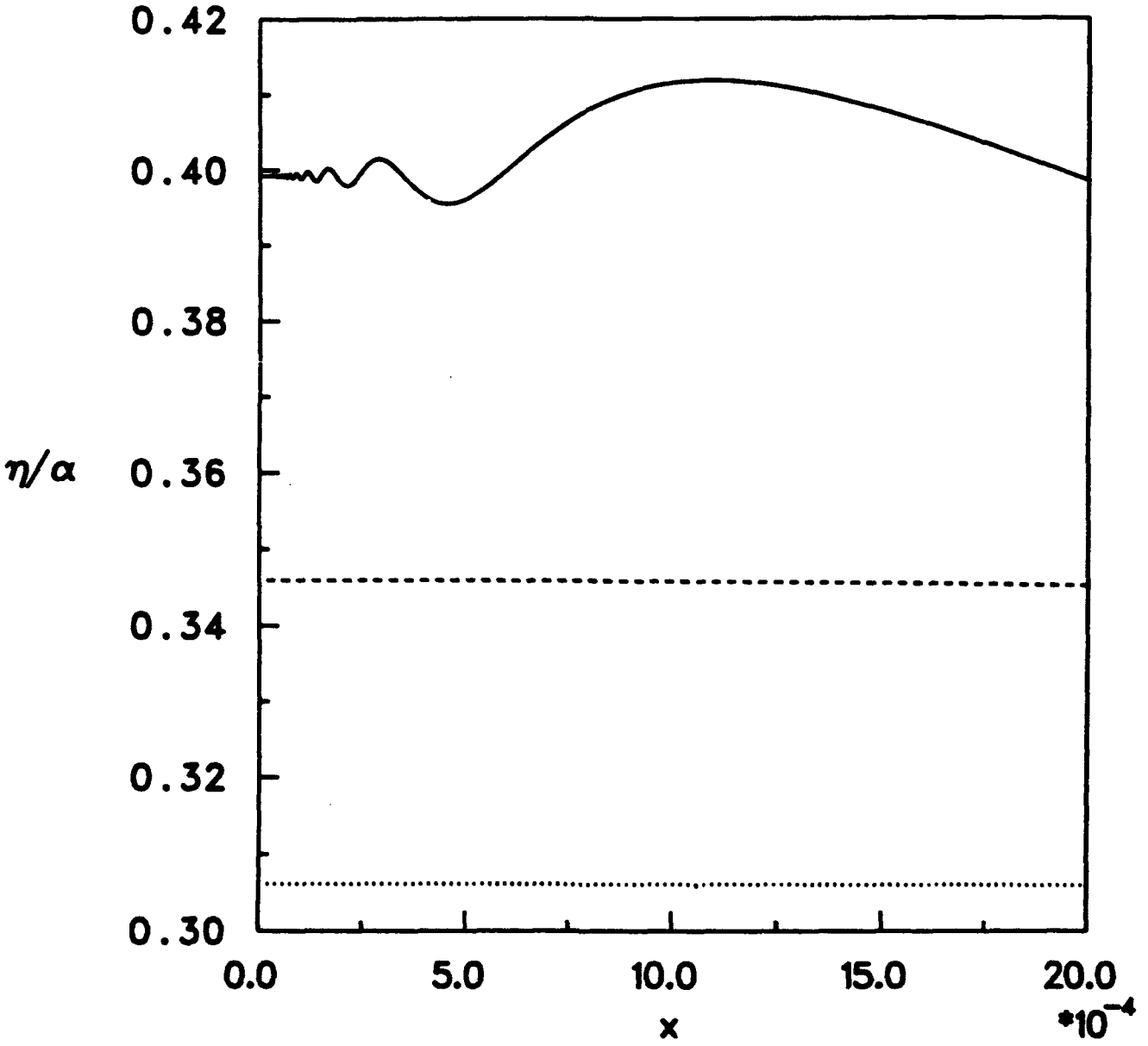

Fig. 4b

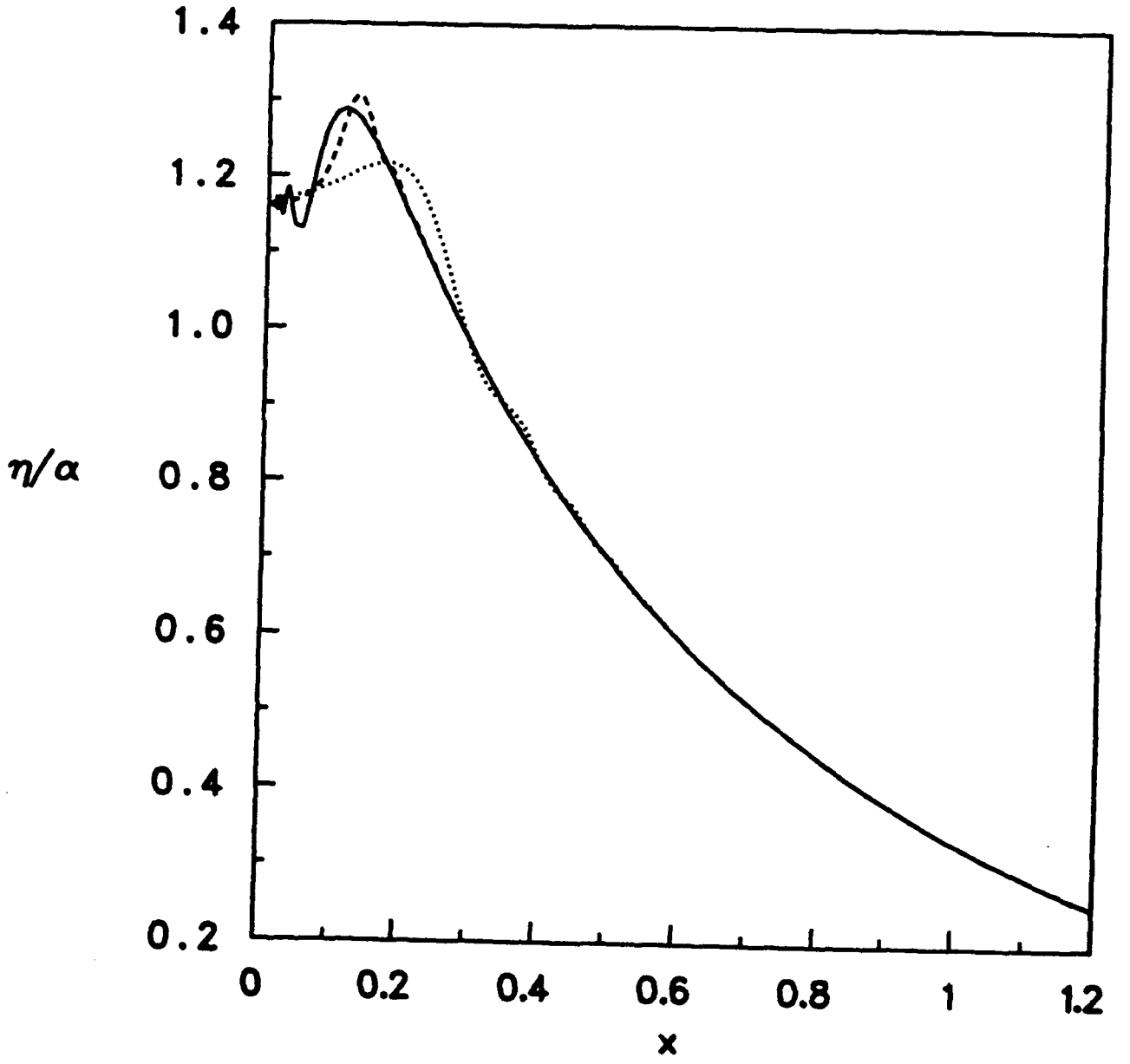

Fig. 4c

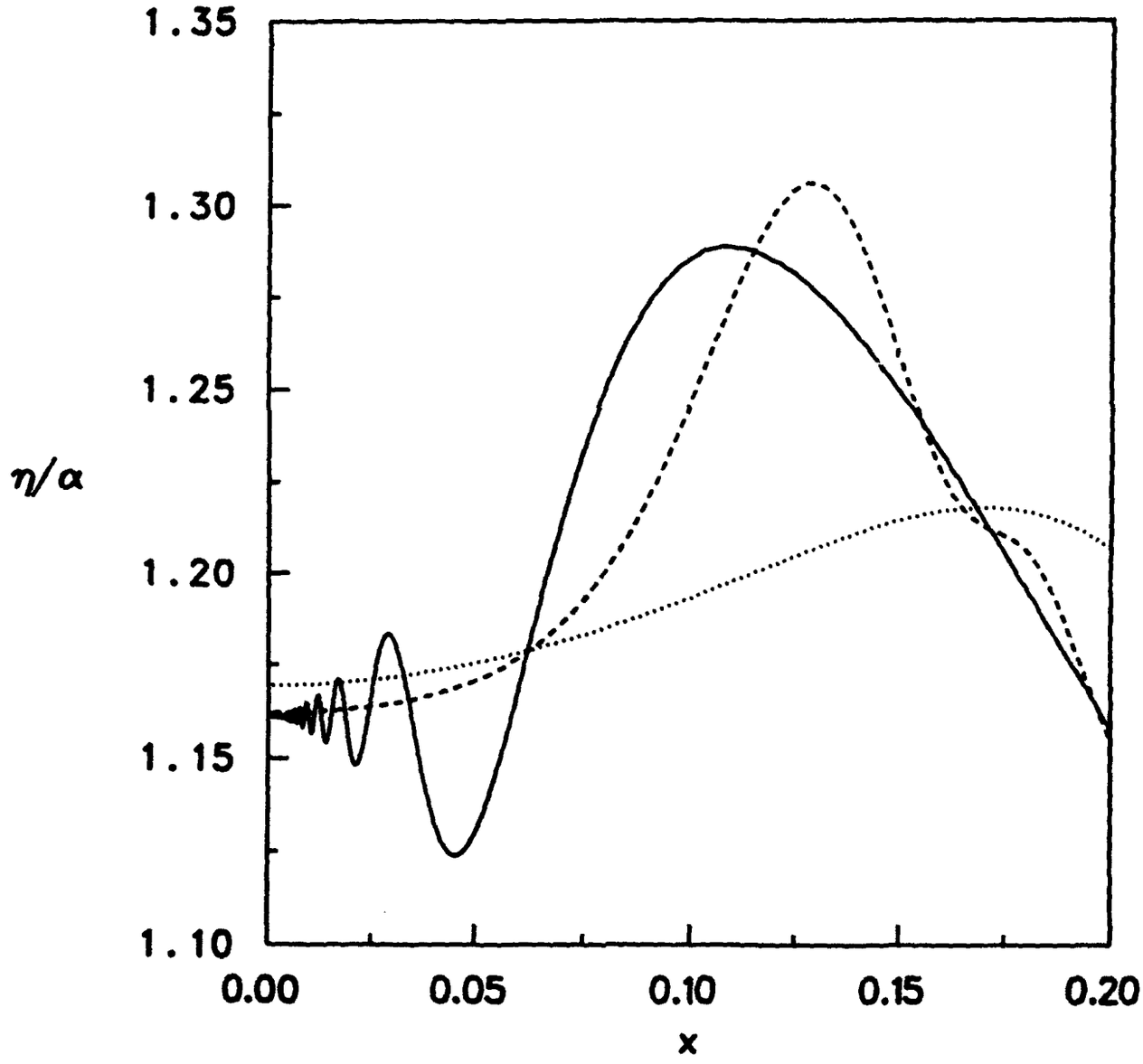

Fig. 4d

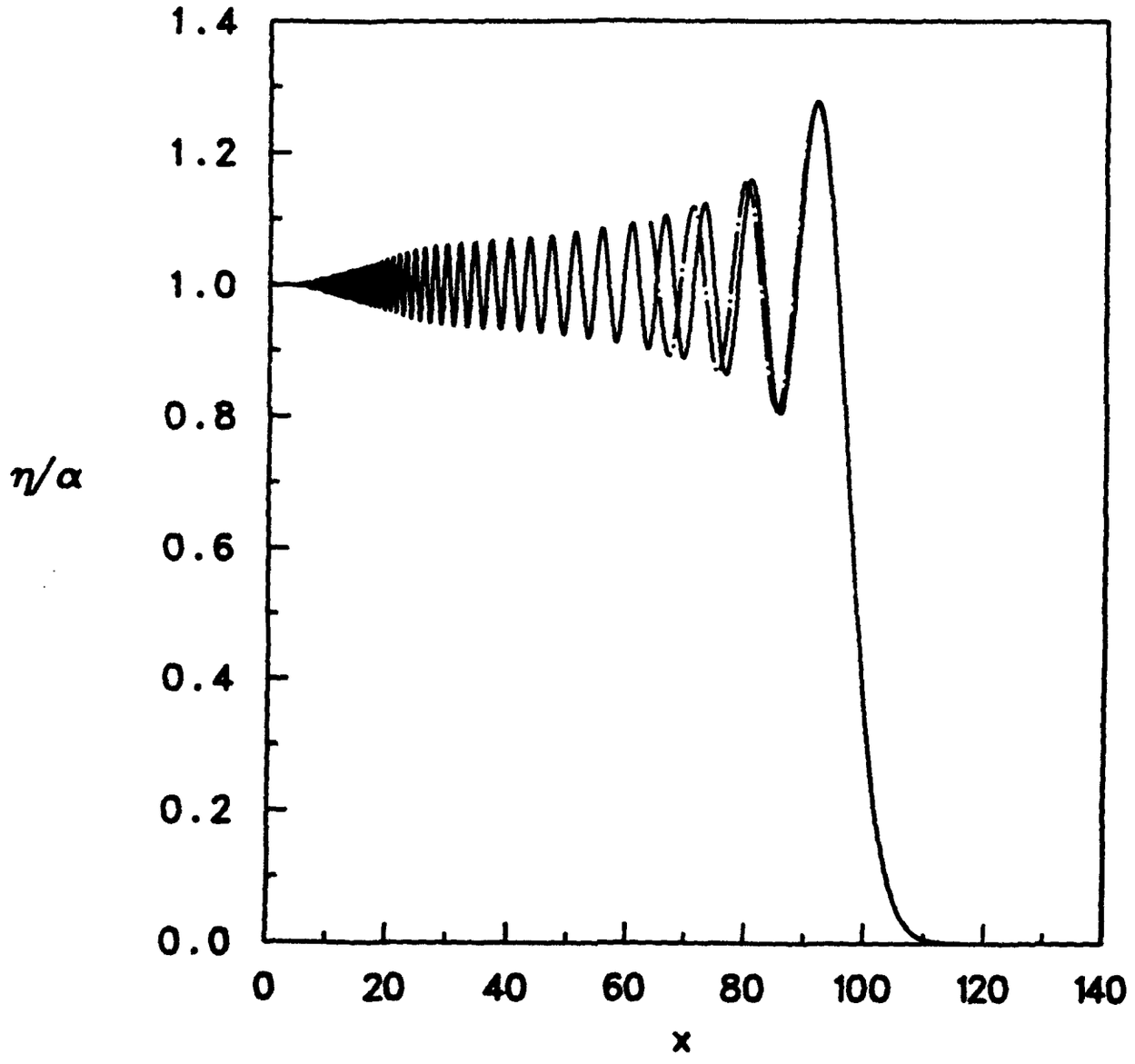

Fig. 40

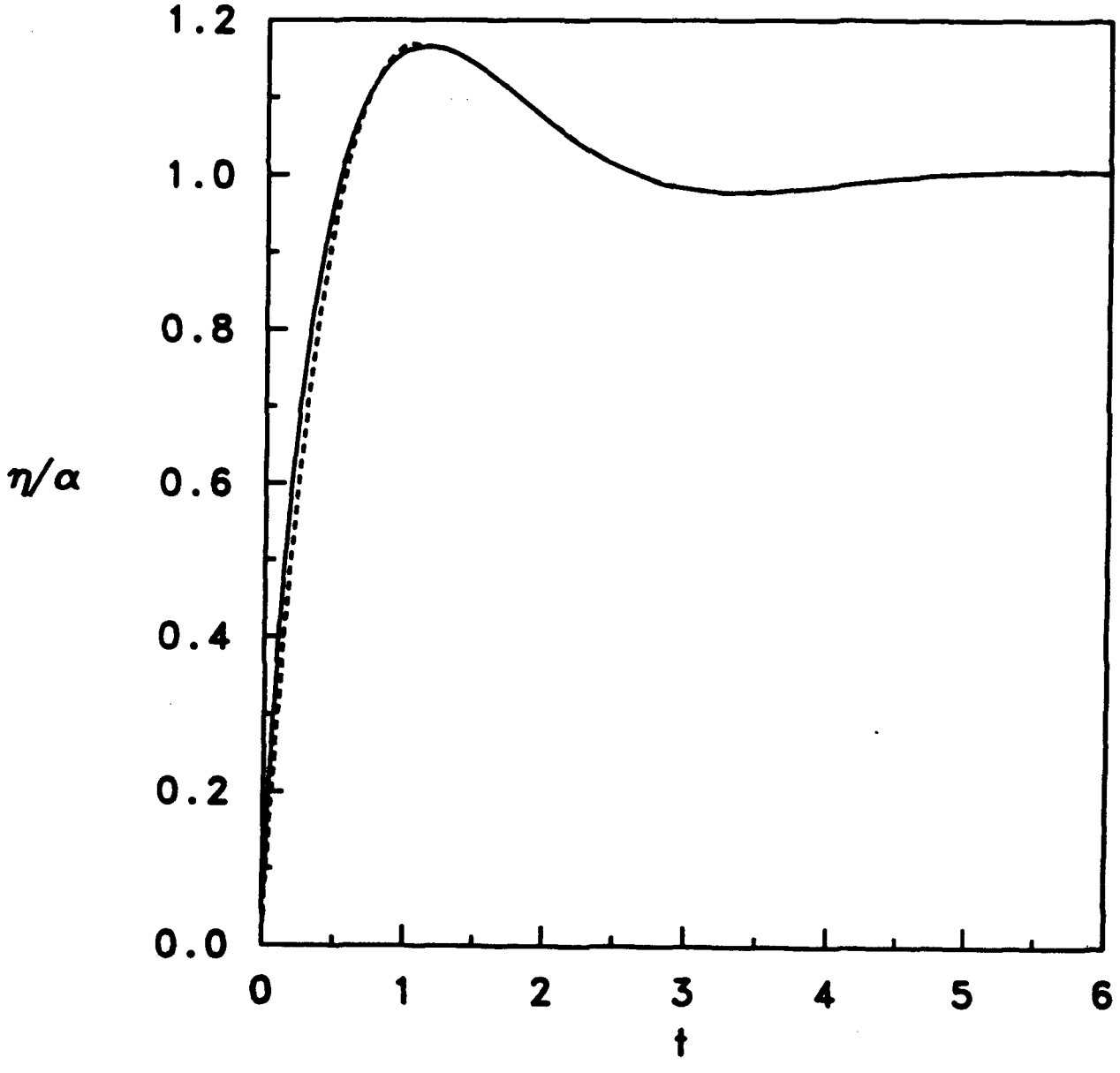

Fig. 5

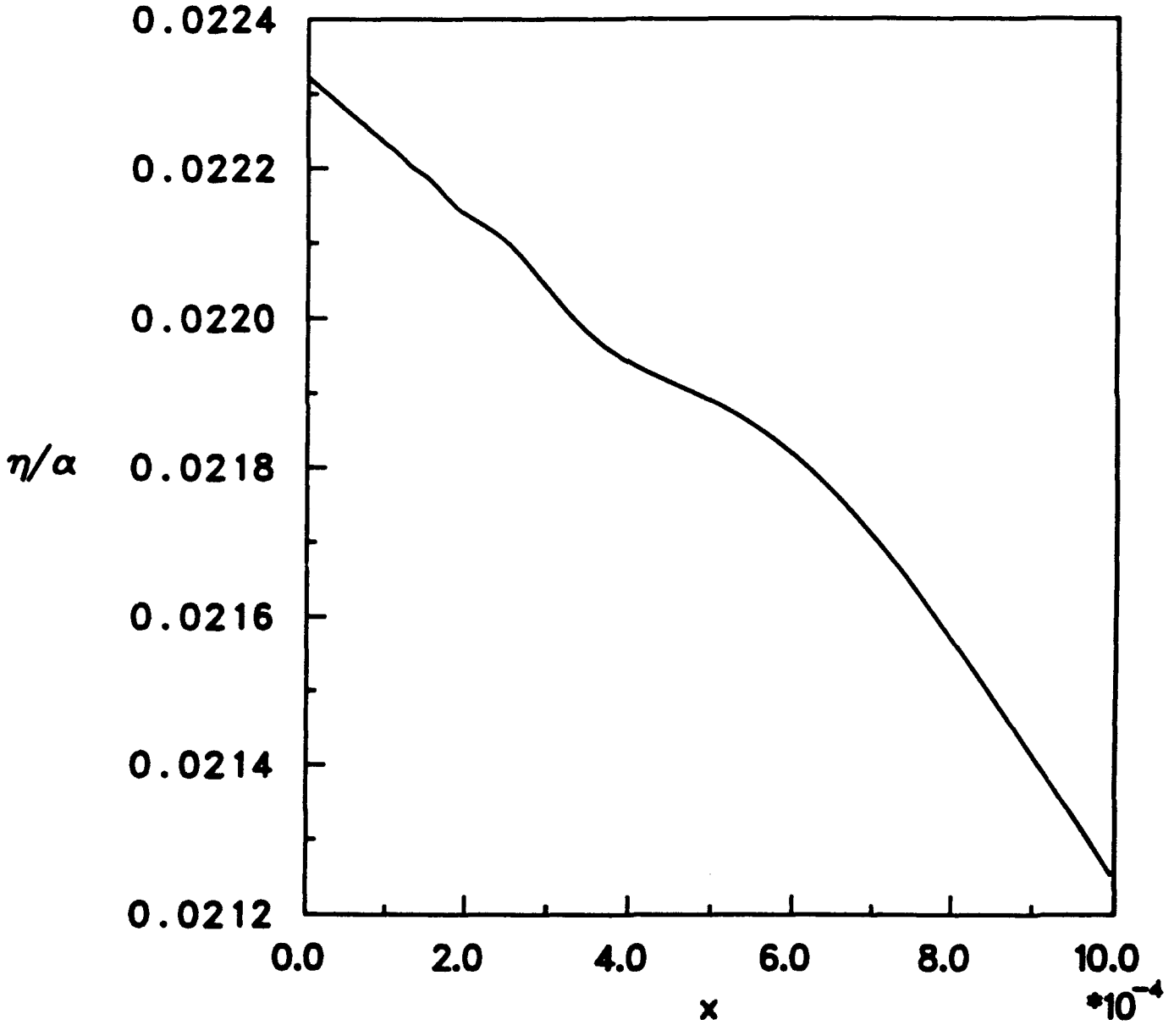
0.0224
0.0222
0.0220
0.0218
0.0216
0.0214
0.0212
η/α
0.0
2.0
4.0
6.0
8.0
10.0
x
*10⁻⁴

Fig. 6a

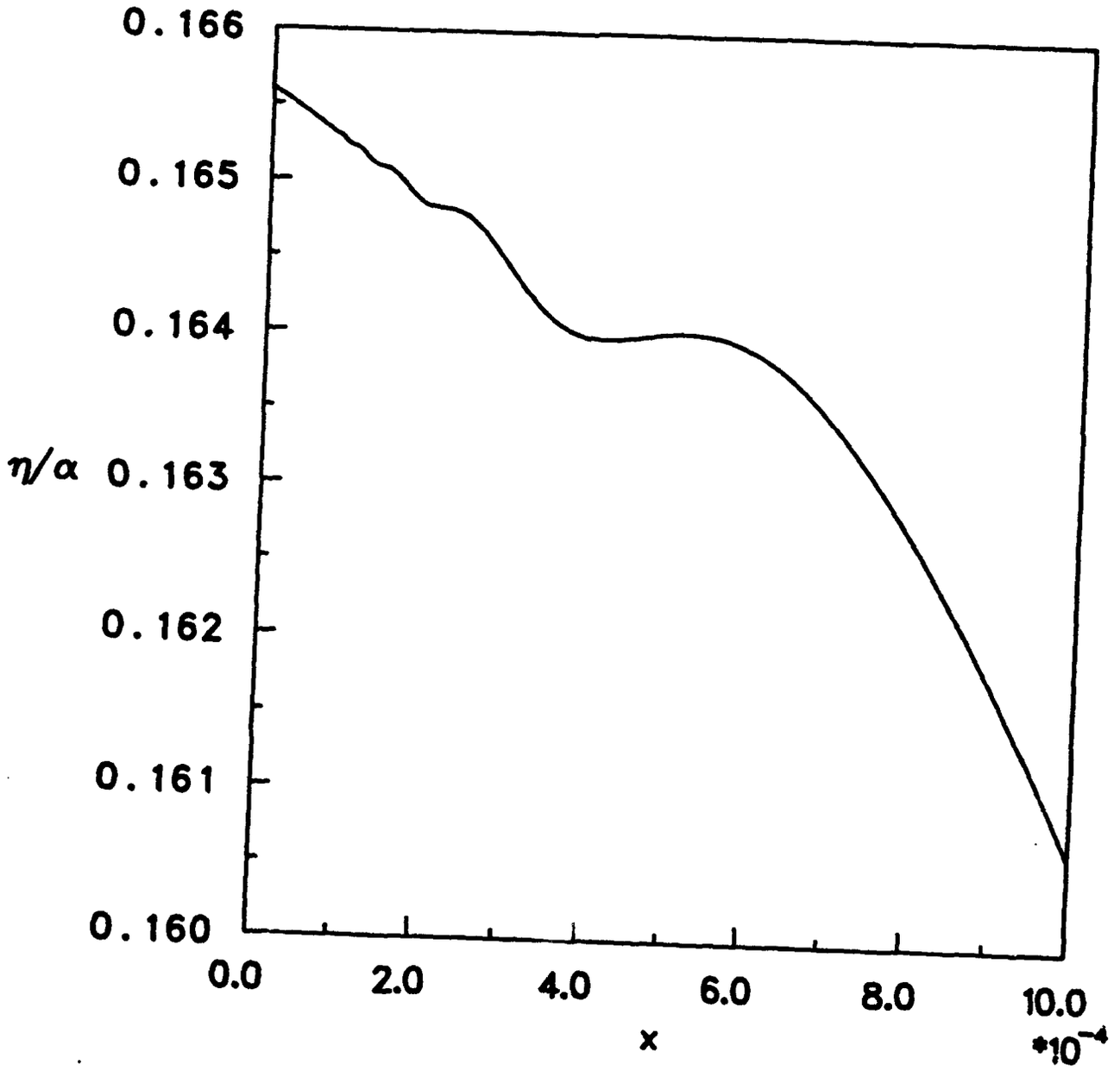

Fig. 6b

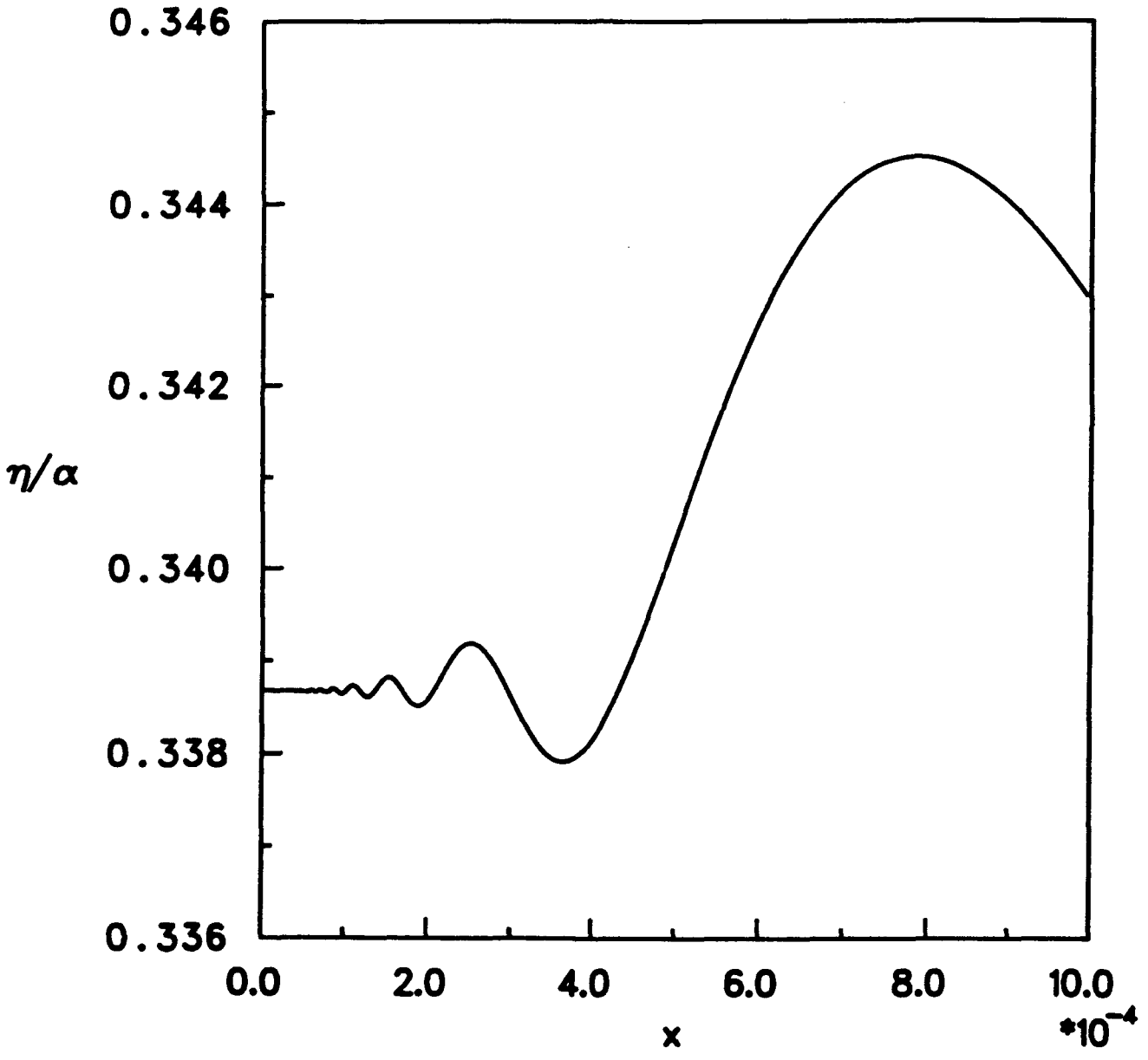

Fig. 6c

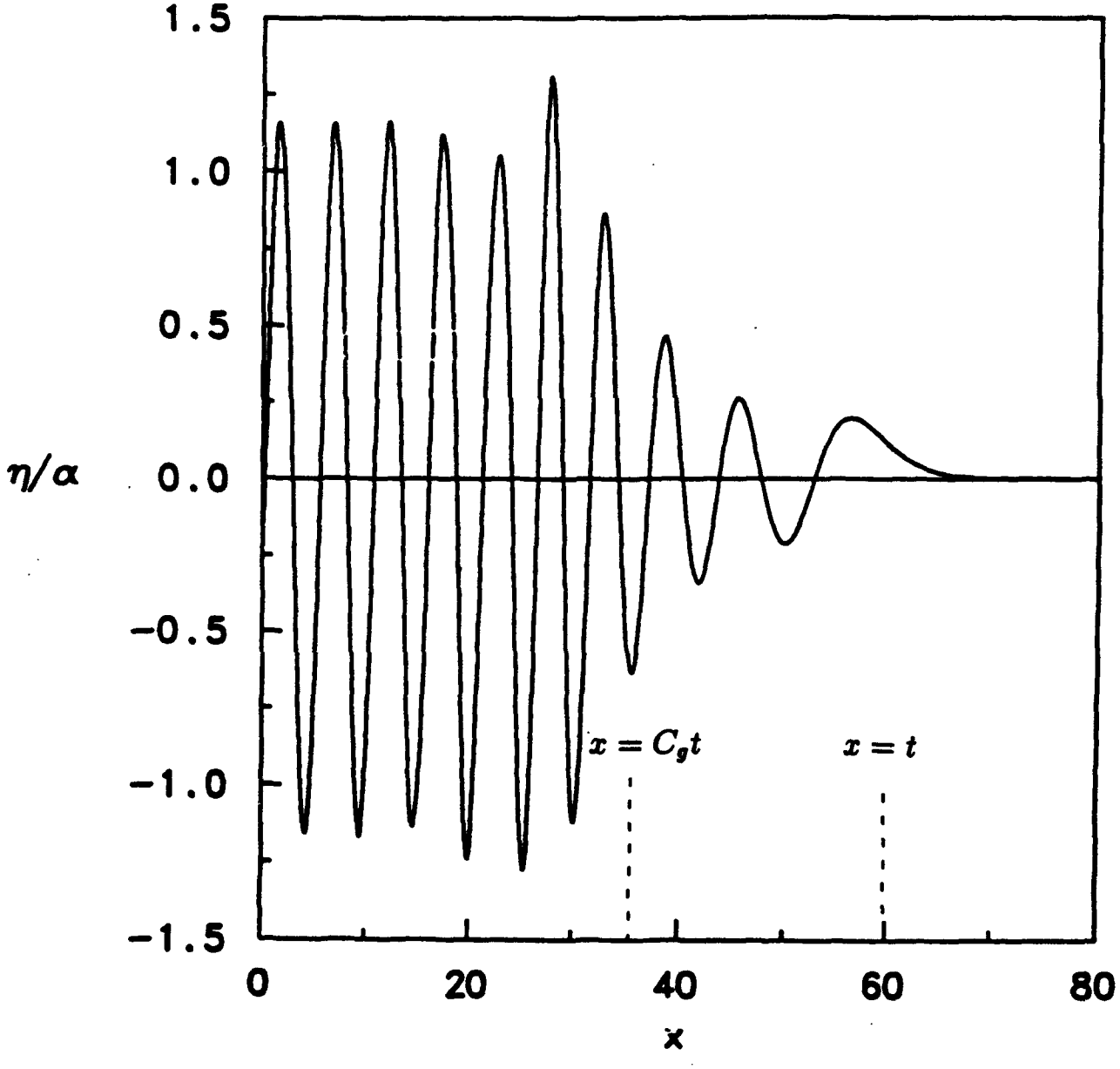

Fig. 7a

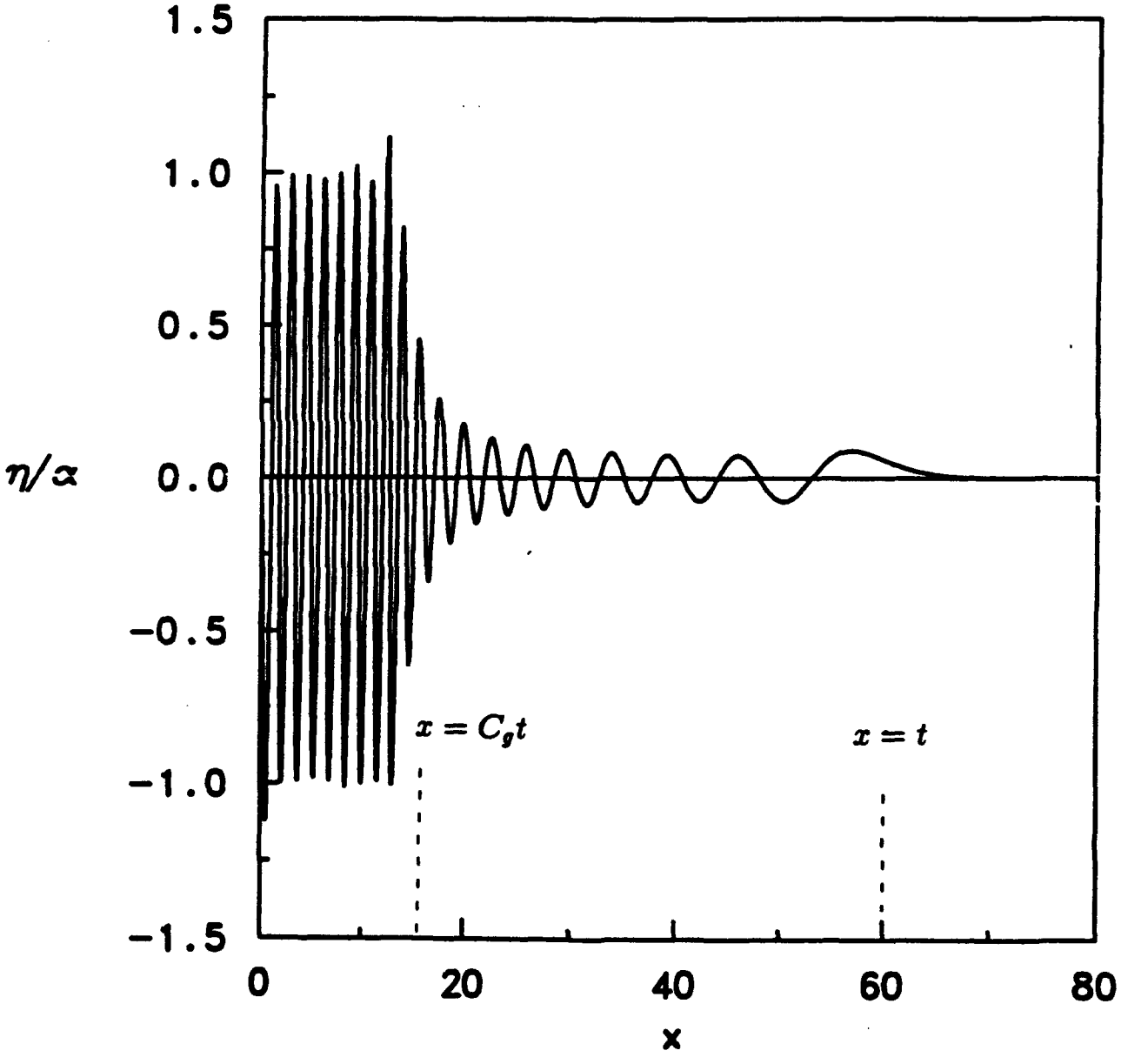

Fig. 7b

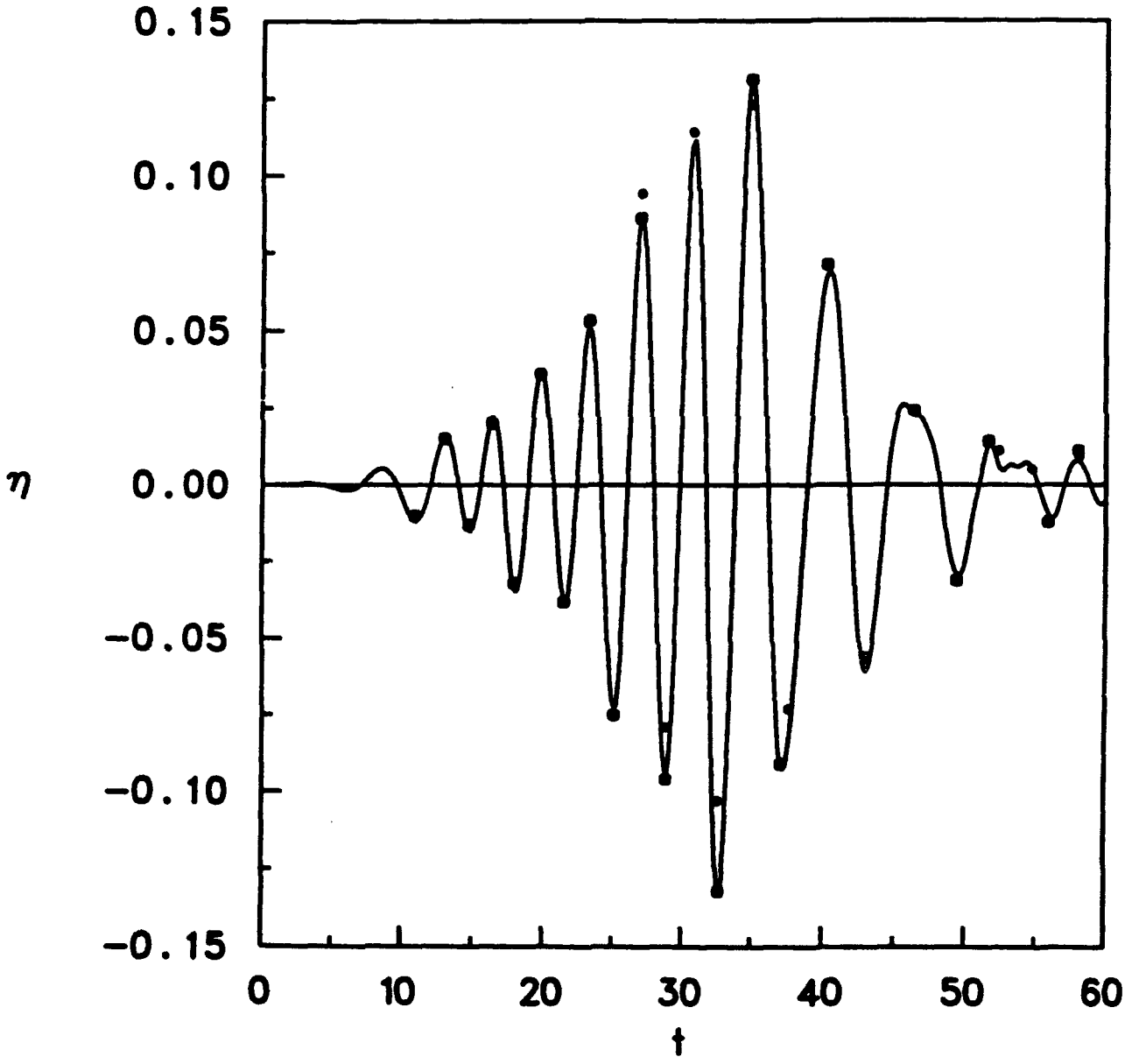

Fig. 8a

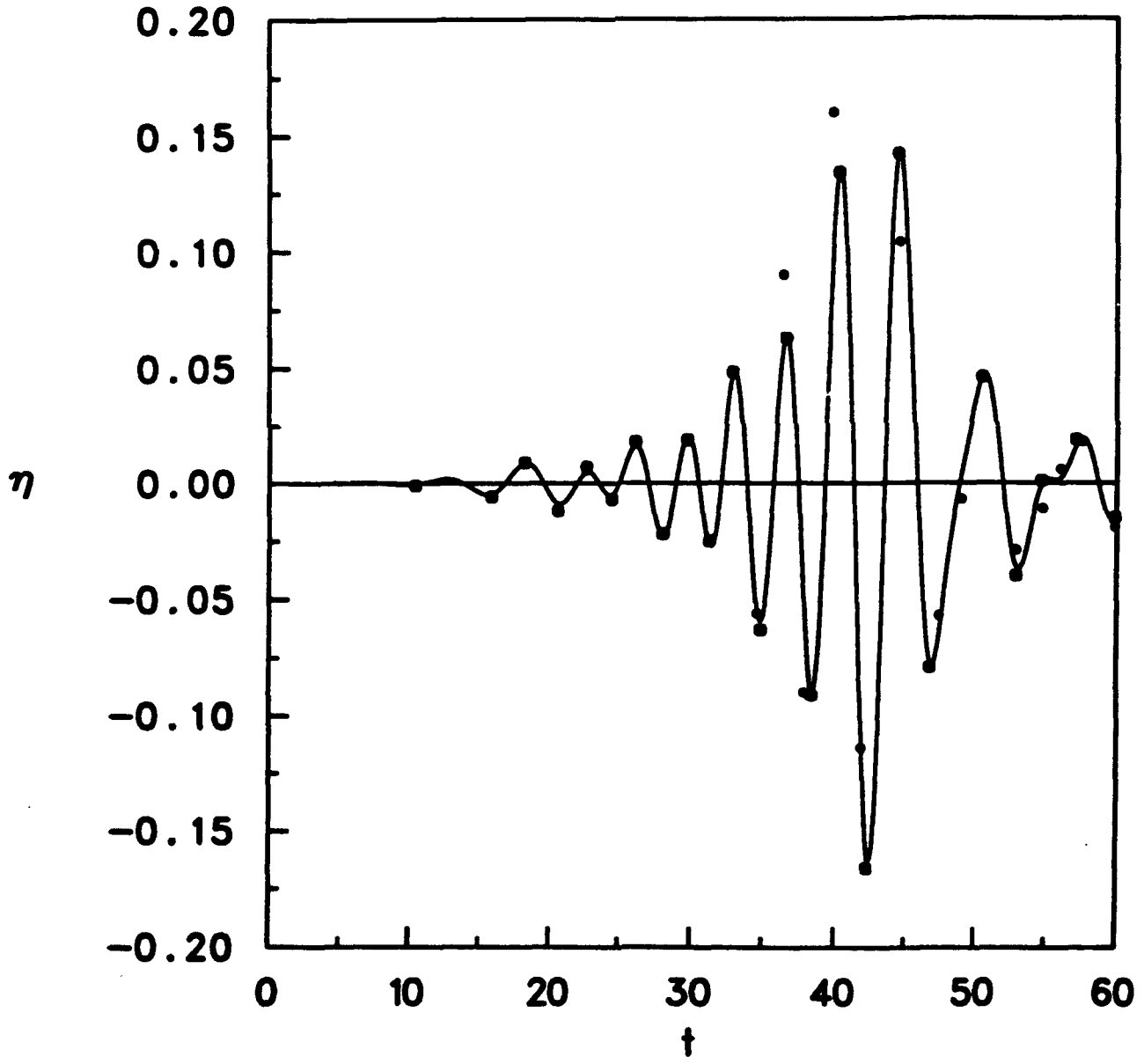

Fig. 8 b

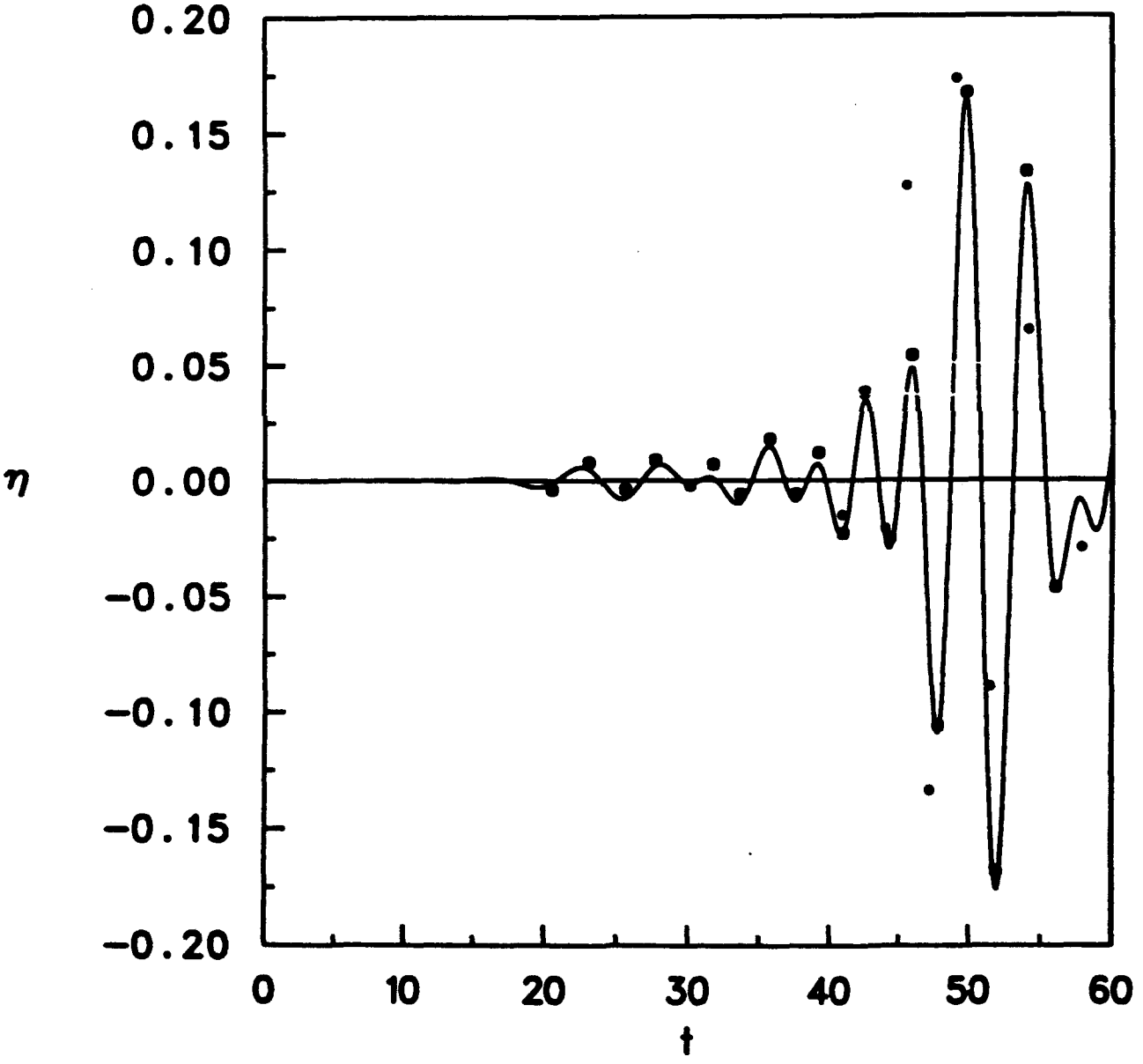

Fig. 8c